UNIVERSIDADE
BEIRA INTERIOR

Design, Construction, and Testing of a Gasoline Valveless Pulsejet Engine

Ana Teresa Rodrigues de Almeida Santos

Dissertação para obtenção do Grau de Mestre em

Engenharia Aeronáutica

(Mestrado Integrado)

Orientador: Prof.º Doutor Francisco Miguel Ribeiro Proença Brójo

janeiro de 2024

Declaração de Integridade

Eu, Ana Teresa Rodrigues de Almeida Santos, que abaixo assino, estudante com o número de inscrição 41462 do Mestrado de Engenharia Aeronáutica da Faculdade de Engenharia, declaro ter desenvolvido o presente trabalho e elaborado o presente texto em total consonância com o **Código de Integridades da Universidade da Beira Interior**.

Mais concretamente afirmo não ter incorrido em qualquer das variedades de Fraude Académica, e que aqui declaro conhecer, que em particular atendi à exigida referenciação de frases, extratos, imagens e outras formas de trabalho intelectual, e assumindo assim na íntegra as responsabilidades da autoria.

Universidade da Beira Interior, Covilhã 22/01/2024

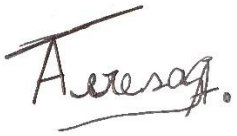

Dedication

To my beloved parents, Pedro, and Adelina.

Acknowledgments

When developing a thesis with an experimental component, we are confronted with the need to integrate not only theoretical aspects but also ones in our approach. In this context, the quest for success relies on the knowledge, advice, and teachings of experienced masters of the craft.

With this, I express my gratitude to my advisor, Professor Francisco Brójo, for the trust in accepting me into this dissertation project. It is with appreciation that I acknowledge the support, guidance, availability, and above all, the knowledge shared with me.

I also thank the laboratory technicians, Engineer João Antunes, Engineer Pedro Oliveira, and Engineer Rafael Domingues, for their support during the experimental phase. In recognition, I express gratitude to Professor José Salvado for providing the code that aided in determining the actual motor frequency and for all the shared knowledge.

Furthermore, I would like to thank the company *Inaceinox, SA*, and Engineer Abel Oliveira for providing all the materials and facilitating the production of Pulsejet. I also thank Master José Rebelo for his work and dedication in the construction process. A special thanks to Engineer Pedro Almeida for assistance in all phases of the project and for valuable advice.

Thanks to my friend Diogo Silva for the assistance throughout the process, but especially for the friendship that will endure.

Last but not least, I extend my thanks to my entire family for their constant support. In particular, to my parents for their patience, upbringing, and constant encouragement.

Resumo

O interesse pelos motores pulsojato foi reacendido especialmente com o crescimento de novas tecnologias na indústria aeronáutica. Este tipo de propulsão foi muito utilizada na Segunda Guerra Mundial, no entanto o elevado ruído e as vibrações excessivas levaram a que a aplicação destes motores na aviação civil fosse descartada. Contudo, devido ao seu design simples e leve têm impulsionado a implementação do pulsojato no mercado de Veículos Aéreos Não Tripulados (UAV's). A natureza complexa dos processos envolvidos neste motor a jato torna a análise fragmentada, exigindo uma compreensão mais aprofundada sobre o seu funcionamento. Assim, de forma a contribuir para a desmistificação do funcionamento deste tipo de propulsão, foi realizado um estudo prático no Departamento de Ciências Aeroespaciais da UBI, sobre um pulsojato sem válvulas do tipo Chinês.

A presente dissertação, investigou o comportamento de um pulsojato sem válvulas quando alimentado a combustível líquido e gasoso, possibilitando a comparação em ambos os cenários. Foi realizado um teste para propano e três testes para gasolina, variando o caudal mássico debitado. Esta investigação permitiu também projetar e construir um sistema de injeção capaz de atomizar o combustível líquido. Ainda assim, o motor a funcionar com gasolina foi menos eficaz do que quando operado com propano. Os valores de TSFC para gasolina foram superiores a 1 kg/N.h e para o teste de propano a taxa de consumo de combustível para alcançar a tração medida foi apenas de 0,574 kg/N.h.

Durante cada teste, os dados relativos à força de tração, temperatura de admissão, temperatura de escape e frequência operacional foram registados. Todos parâmetros, nos ensaios a gasolina, diminuíram devido às características específicas da gasolina, nomeadamente à velocidade de queima, mas sobretudo à pressão de injeção. O queimador de combustível líquido necessitava de mais pressão para fragmentar a gasolina em partículas menores, de forma a melhorar a interação entre o combustível e o ar. Contudo obteve-se o efeito autossustentável tanto com o motor a funcionar a propano como a gasolina, embora tenha sido observada uma combustão instável nesta última.

Palavras-Chave

Pulsojato; Pulsojato sem válvulas; Pulsojato tipo Chinês; Combustível Líquido; Gasolina; Bico Queimador de Combustível Líquido; Atomização

Abstract

Interest in pulsejet engines has been reignited, especially with the growth of new technologies in the aeronautical industry. This type of propulsion was extensively used during World War II; however, its application in civilian aviation was discarded due to high noise levels and excessive vibrations. Nonetheless, owing to its simple and lightweight design, it has propelled the implementation of pulsejet engines in the Unmanned Aerial Vehicles (UAVs) market. The complex nature of the processes involved in this jet engine makes the analysis fragmented, demanding a deeper understanding of its operation. Thus, to contribute to the demystification of this type of propulsion, a practical study was conducted at the Department of Aerospace Sciences at UBI on a valveless Chinese-type pulsejet.

The present dissertation investigated the behaviour of a valveless pulsejet when fueled by liquid and gaseous fuel, allowing for comparison in both scenarios. One test was conducted using propane, and three tests were carried out using gasoline, varying the mass flow rate. This research also involved designing and constructing an injection system capable of atomizing the liquid fuel. However, the engine operating with gasoline was less efficient than when operated with propane. The TSFC values for gasoline exceeded 1 kg/N.h, while for the propane test, the fuel consumption rate to achieve the measured thrust was only 0.574 kg/N.h.

During each test, data regarding thrust force, intake temperature, exhaust temperature, and operational frequency were recorded. All parameters in the gasoline tests decreased due to the specific characteristics of gasoline, particularly the burning speed, but mostly due to the injection pressure. The liquid fuel burner required more pressure to break the gasoline into smaller particles to improve the interaction between the fuel and the air. Nonetheless, the self-sustaining effect was achieved with both the propane and gasoline-operated engines, although unstable combustion was observed in the latter.

Key Words

Pulsejet; Valveless Pulsejet; Chinese type Pulsejet; Liquid fuel; Gasoline; Oil Burner Nozzle; Atomization

Index

List of Figures

List of Tables

List of Acronyms

CAD	*Computer-Aided Design*
CFD	*Computational Fluid Dynamics*
CNC	*Computerized Numerical Control*
EMF	*Electromotive Force*
LAMV	*Light Aerial Multipurpose Vehicle*
PDE	*Pulse Detonation Engine*
PETA	*Pulse Ejector Thrust Augmenter*
TIG	*Tungsten Inert Gas*
UAV	*Unmanned Aerial Vehicles*
USAAF	*United States Army Air Force*
VTOL	*Vertical Take-Off and Landing*

List of Symbols

c	*Speed of Sound*	*[m/s]*
c_a	*Admission Sound Speed*	*[m/s]*
c_e	*Exhaust Sound Speed*	*[m/s]*
C_{P_c}	*Specific Heat at Constant Pressure (cold)*	*[J/(kg.K)]*
C_{P_h}	*Specific Heat at Constant Pressure (hot)*	*[J/(kg.K)]*
F	*Thrust*	*[N]*
f	*Pulsejet Frequency*	*[Hz]*
f_a	*Pulsejet Admission Frequency*	*[Hz]*
f_e	*Pulsejet Exhaust Frequency*	*[Hz]*
M	*Mach Number*	*[-]*
L	*Pulsejet Length*	*[m]*
L_a	*Pulsejet Admission Length*	*[m]*
L_e	*Pulsejet Exhaust Length*	*[m]*
$\dot{m}_a$	*Air Mass Flow*	*[g/s]*
$\dot{m}_f$	*Fuel Mass Flow*	*[g/s]*
P	*Pressure*	*[Pa]*
Q_R	*Fuel Heating Power*	*[J/kg]*
$r_{c/a}$	*Ratio between Mass Flow Rate of Fuel and Air*	*[-]*
S_a	*Cross-sectional area of the intake duct*	*[m²]*
T	*Temperature*	*[K]*
TSFC	*Thrust Specific Fuel Consumption*	*[kg/(N.h)]*
U	*Flight Speed*	*[m/s]*
U_e	*Exit Speed*	*[m/s]*
V	*Volume*	*[m³]*
V_{cc}	*Combustion Chamber Pulsejet Volume*	*[m³]*

Chapter 1

1. Introduction

1.1. Motivation

With advancements in the aeronautical industry, various technologies have emerged to enhance engine efficiency and minimize losses. However, the choice of the engine type must consider factors like production costs, emissions, available technologies, etc., leading to the development of four common propulsion systems for aircraft: Turbojet, Turboprop, Propellers (piston-prop), and Turbofan. Despite their good performance, these systems are complex and require meticulous maintenance.

During World War II, the pulsejet engine emerged as an intermediate concept between piston and gas engines, operating in pulses. While less efficient than constant-volume propulsion devices, pulsejets suffered from slow reaction rates limiting operating frequency, pressure rise, and specific impulse. Excessive fuel consumption, vibrations, and noise led to its removal from civil aviation [1].

Although the reasons for its limited development are unclear, interest in pulsejet engines has been reignited, especially with the growth of UAV technology. Despite the focus on electric propulsion in various aviation fields, energy storage limitations still hinder its implementation for certain missions requiring higher power density.
As a result, pulsejet propulsion is being considered due to its simple, lightweight design, demonstrated performance, and advancements in lightweight, high-temperature resistant materials.

1.2. Goals of the Investigation

The present investigation is essentially a continuation of two previous dissertation projects conducted in the Department of Aerospace Sciences at UBI. These earlier works involved the sizing, numerical analysis, and subsequent construction of a valveless pulsejet utilizing propane as the fuel. In contrast, the current project is focused on developing a model with optimized geometry, employing liquid fuel.

One of the primary objectives is to devise an effective and appropriate injection system tailored to this specific case study. Moreover, the project aims to experimentally assess operational parameters under different flow rates. Additionally, tests will be conducted

using gaseous fuel primarily aimed at analysing geometries and verifying improvements made to the previous pulsejets. This approach allows for a comparative analysis of data obtained from experimental tests conducted with gaseous fuel, enabling the evaluation of the performance of the new model utilizing gasoline as the energy source. It is also possible to compare the data with the literature, allowing for an examination of any deviations from theoretical expectations and an exploration of the phenomena that any given rise to such differences.

Initially, this dissertation will entail an in-depth research phase focusing on technical literature to comprehend the principles of pulse propulsion. The goal is to enhance the understanding of pulsejet engine behaviour. This literature review will prove highly valuable for decision-making processes. Subsequently, when acquiring data from the examined propellant, there will be an opportunity to validate certain theoretical concepts outlined in the bibliography.

The aspiration is to acquire experimental data using a set of strategically placed sensors capable of recording real-time operational parameters. To accomplish this, there is an intention to develop an efficient and comprehensible code for future use.

Ultimately, it is intended to describe all procedures, decision-making processes, and outcomes to facilitate analysis in conjunction with the theoretical component.

1.3. Methodology and Structure

To accomplish the specified objectives, this dissertation is structured into six chapters. The current chapter provides a contextualization of the planned research, outlining the motivation, methodology, and adopted structure.

In Chapter 2, an initial historical overview is provided to contextualize the emergence of the pulsejet engine, spanning from its inception to the latest models. Several examples of engines and aircraft are included for enhanced contextual understanding. Subsequently, a comprehensive review of the state of the art is presented, incorporating various scientific studies. These investigations offer insights into the functioning of pulsejet engines and provide avenues for improvement, outlining their consequential impact on the performance of these propulsion systems.

In Chapter 3, a classification of diverse pulse engines is conducted, accompanied by an exposition of the pulsejet engine concept. Theoretical concepts pertaining to the operation and performance of a valveless pulsejet engine are delineated. This theoretical component facilitates an understanding of the operation of deflagration pulse engines and the calculation of specific performance parameters.

In Chapter 4, the entire experimental procedure is described. Firstly, the initial design of the engine is detailed, along with materials and manufacturing processes employed in the construction of the pulsejet. Additionally, supplementary systems for motor operation are introduced. Moreover, some operational challenges are revealed, necessitating adjustments from the initially envisioned plan.

In Chapter 5, an enumeration of the diverse sensors employed for practical data acquisition is provided. This chapter comprehensively presents and discusses all obtained experimental results.

In the final chapter (Chapter 6) of this dissertation, a comprehensive evaluation of the conducted research is performed, and the relevant conclusions are presented. Additionally, recommendations for future work are put forth, suggesting areas that could be explored after this study.

Chapter 2

2. Literature Review

2.1. Brief History

The idea of pulse combustion emerged at the end of the 17th and beginning of the 18th century, in which the investigations of Huygens and Allen contributed significantly to the use and application of this technology [2]. These references generally deal with complex fluid-thermo-chemical processes to control the operation of these engines.

However, most of the developments started at the beginning of the 20th century. Martin Wiberg developed the first pulsejet in Sweden, but it was only in 1906 that V.V. Karadovin officially obtained a patent. In 1907 the first pulsejet was built in Russia, which was a high-speed jet whose liquid hydrocarbon fuel/air mixture was injected by pulses in a gaseous state.

In 1907, a new version of the pulsejet was created by Georges Marconnet (see Figure 2.1). This new version had no valves and was composed of an intake diffuser, a combustion chamber, and an extensive exhaust nozzle to expel the gases resulting from combustion.

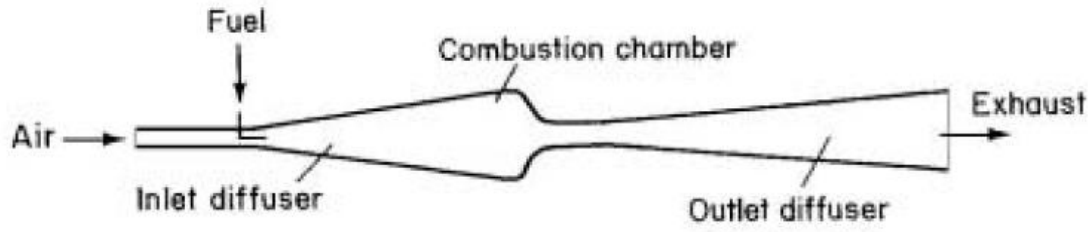

Figure 2.1-Marconnet's Pulsejet Engine [4].

In 1939 the German designer Paul Shmidt designed a valved pulsejet. Eight years later, with the improvement of the Argus company, it was manufactured, and in December 1942 the first flight of the V-1 “Buzz Bomb” was carried out. The Schmidt Argus V-1 pulsejet engine is the most famous pulsejet engine in history and was extensively used in bombing raids against England and Belgium in World War II [1].

The “Buzz Bomb”, so named due to the high noise, was an unmanned bomb weighing more than two tons, including 80-octane gasoline and an 850 kg warhead. The aircraft was powered by a pulsejet engine producing 2900 N of thrust at an altitude close to 1 km. This simple jet engine completed around 500 combustion cycles per minute, giving the flying bomb a cruising speed of over 640 km/h. The propulsive system was placed on the fuselage (see Figure 2.2).

It was launched on a ramp, inclined 46 m, and was driven by a gyroscope, which collided with the ground when the fuel was extinguished, making an average of 240 km. It was also common to drop the bomb from a cargo aircraft (usually He III Hs of KG 3 and later KG 63) [3].

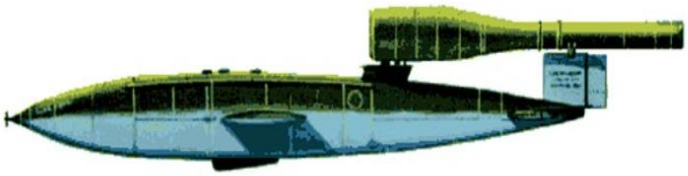

Figure 2.2-V-1 "Buzz Bomb"[3].

In July 1944, some wreckage was captured by the US Army, where the USAAF and American industry built their own V-1, more known as "Jet Bomb 2 (JB-2)", equipped with a pulsejet engine designated PJ-31 produced by Ford [1]. The JB-2's launch conditions were like the V-1, it needed a slipway with an auxiliary solid fuel propellant attached on board or it was launched via bombers. The US Navy manufactured a new variant of the V-1, the “KUW-1 Loon”. After initial trials in 1946, the submarine USS CUSK was modified for the launch of Loon flying bombs. The flying bomb was stored in a watertight reservoir and launched by solid rocket boosters while the submarine was on the surface.

Many other countries tried their version of the V-1. In 1944 Japan built the Yokosuka MXY7 Ohka, an aircraft with a propulsive system identical to the V-1, for suicide missions against the Allied naval forces. These aircraft were transported by bombers (G4M “Betty”) and then guided by pilots to their final destination [1].

In the early 1940s, US Navy Lieutenant William Schubert modified Marconnet's pulsejet, designated the "resojet", represented in Figure 2.3. Major advances over Marconnet’s technology were the sudden expansion of the combustion chamber inlet and the new intake design. Due to the abrupt variation of the section in the combustion chamber, it was possible to generate greater turbulence and, therefore, increase the mixing capacity of the air/fuel flow, that is, make the combustion more efficient. The new intake design prevented post-combustion gases from escaping before the internal pressure of the combustion chamber was below atmospheric.

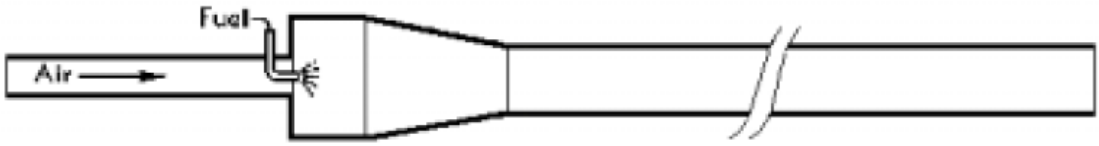

Figure 2.3-Schubert's Pulsejet Engine [4].

In the 1950s, France developed a drone based on V-1 technology, designated the “Arsenal 5501”. This was guided by a radio system that had twin tail fins.
In the same decade, a group of engineers from the company SNECMA (France) developed the Escopette engine (see Figure 2.4). This engine was a valveless pulsejet, in which the intake was facing backward, providing a considerable increase in thrust by the flow reversal effect. Another peculiarity of this engine was the propulsive nozzle, which was segmented into different stages of an increasing section, giving rise to different waves of compression and rarefaction for each explosion cycle [4].

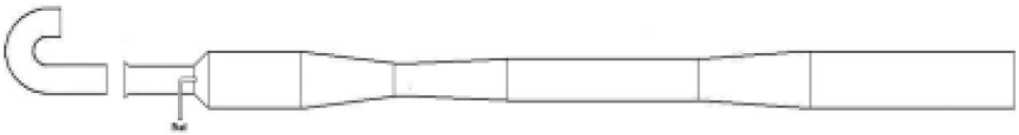

Figure 2.4-The French "Escopette" valveless pulsejet [4].

In the early 1960s, a study began for the development of all potential sources of jet propulsion available at the time. Under the initial direction of J.G. Logan at the Cornell Aeronautical Laboratory, several valveless pulsejet designs were tested. In this project, several geometries were developed and their performance with hydrocarbon fuels was analysed. Due to this analysis, the efficiency of each cycle and the heat release rate were improved.

In the same decade, Lockwood, in collaboration with Hiller company, began investigating valveless pulsejet reactors for lift-propulsion systems. Several concepts were designed, produced, and tested, but the one that performed best was the “U” shaped pulsejet [5]. This is considered the most effective pulsejet ever created. A peculiarity of this engine is the fact that it does not have any part of a constant section along its structure, the admission is made through the shorter straight tube, while the curved nozzle serves for the exhaust gases (see Figure 2.5). This non-uniform cross-section brought some improvements when compared to engines at the time. Another notable feature of the Lockwood engine was the installation of traction boosters, both in front of the intake and at the end of the exhaust nozzle, thus increasing the output of the pulsejet.

The afterburner employed the heat from exhaust gases to draw in ambient air, thereby enhancing traction. In the case of on military-specific model (HH 5.25-7) it generated a maximum traction force of 1335 N.

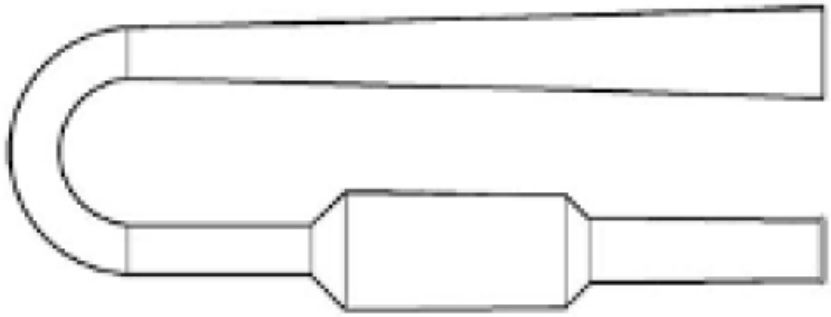

Figure 2.5- Schematic of the Hiller-Lockwood Pulsejet [4].

Between the 1970s and 1980s, J.A.C. Kentfield added a recuperator, in which he managed to increase the traction generated by the pulsejet. Instead of a backward-bent tube, he applied a smoothly curved cone that allowed cool air to be sucked into the hot gas stream as an extra reaction mass (this is often referred to as the secondary traction boost) [1]. According to Kentfield, this structure compensated for the drag and turbulence losses that occur in a 180° turn.

Kentifield conducted tests on numerous prototypes, with the majority of recuperators being symmetrical and employing internal vanes to manage airflow and reduce turbulence. Figure 2.6 showcases two recuperators that exhibited superior performance. Kentfield's analysis led to the conclusion that the more straightforward design on the right (b) outperformed model (a). This was primarily because a pulsejet engine operates intermittently, resulting in significant losses when fresh air is drawn in a linear path. With the said intake, air acceleration was more efficient [4] [6].

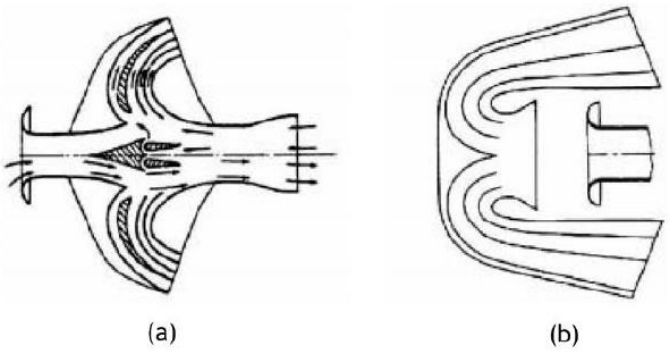

Figure 2.6- Kentfield Recuperator Models (Adapted from [4]).

Currently, new patents have emerged for this type of propulsive system. Boeing is developing a new design called the Pulse Ejector Thrust Augmenter (PETA), as illustrated in Figure 2.7 The American manufacturer proposes the use of valveless pulsejet engines for vertical take-off and landing aircraft (VTOL), both for military and commercial aircraft. Boeing's design incorporates the pulsejet inside a thrust augmenting duct, which draws moving air into the exhaust stream. This movement improves thrust and cools the engine better [7]. Each pulsejet includes a combustion chamber with an upstream inlet port joined to an inlet diffuser and a downstream outlet port joined to a discharge nozzle. Boeing intends to implement this technology on board the LAMV, a prototype aircraft [8].

In the last years, pulsejet engines earned a new interest, particularly for their use in UAV propulsion. Several manufacturers started looking for ways to efficiently source power for long-range UAVs [1]. The main research focuses on pulse detonation engines (PDE). The PDE has a tube that serves as a combustor and where the detonation of the air/fuel mixture is initiated. While conventional pulsejets use deflagration, having subsonic combustion, PDE has supersonic combustion. The detonation wave rapidly passes through the chamber, resulting in a process of adding heat at constant volume, producing a high pressure in the combustor, and thus providing thrust.
These types of engines are structurally simple, have low fuel consumption, and intrinsic capability of operating from zero approach stream velocity to high supersonic flight speeds. Despite these advantages, its operation is not that simple, and the high noise level continues to be one of the obstacles to the application of these engines in certain aircraft [2].

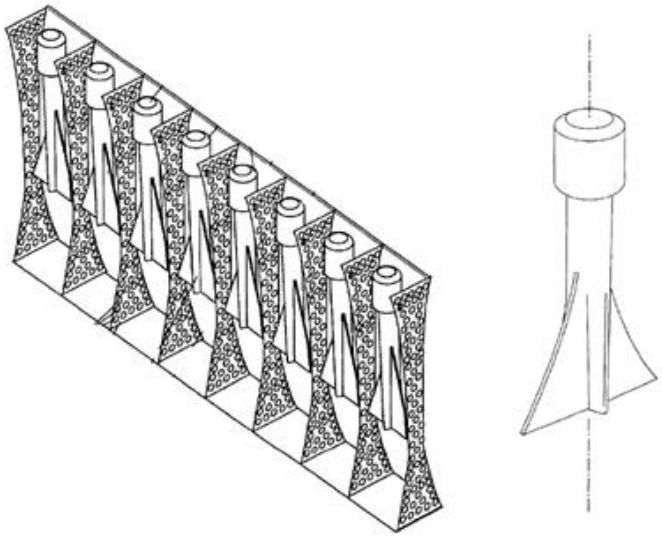

Figure 2.7- Boeing Pulsejet Thrust Augmenter (Adapted from [8]).

2.2. State of Art

The pulsejet engine was an invention of the last century and has lost interest through the years, mainly due to its high noise. However, in recent years new studies have emerged to improve performance for possible applications in the future.

Wenxiang et al. [9] studied the influence of the propulsive nozzle length on the performance of a Chinese-type valveless pulsejet. To this end, they executed numerical simulations of a pulsejet with 830 mm in length in CFD programs, fed with propane gas with a constant mass flow rate of 0.4 g/s.

The authors also intended to study the processes of mass, momentum, energy, and components between the pulsejet and surrounded environment, farfields are set near the inlet and the outlet, respectively (see Figure 2.8).

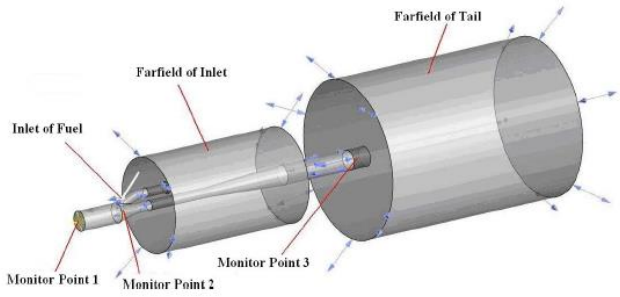

Figure 2.8-Boundaries and monitor points (Adapted from [9]).

The results showed that each cycle lasts 0.004 s and the operating frequency of this pulsejet is 250 Hz. The temperature varies linearly between the combustion chamber and the intake, showing the same behaviour until the exhaust.

The conducted simulations enabled the researchers to deduce that a reduction in the combustion chamber's length correlates with an increase in the pulsejet's frequency. Furthermore, their results corroborate that for cut segments measuring less than 30 mm, the rate of frequency increase is gradual, whereas it accelerates significantly when the cut segment exceeds 30 mm in length.

Tao et al. [10] carried out a study in which a numerical simulation was performed to understand how valveless pulse combustion works and to study the multicycle work process. To this end, a typical valveless pulse combustor, shown in Figure 2.9, was simulated.

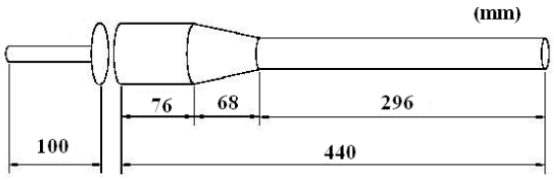

Figure 2.9-Measurements of a typical valveless pulsejet [10].

The author concluded that the primary oxygen consumption within the combustor is attributed to chemical reactions. However, in instances of fuel leakage into the combustor, unburned oxygen persists in the rear of the combustor.
The simulation results, in Figure 2.10, show the variation of the pressure along the time. It is discernible that a secondary pressure peak emerges between two consecutive cycles, indicative of pressure waves within the pulse combustor overlapping and interacting with one another. Notably, the second pressure peak at the exhaust exhibits greater prominence compared to that at the inlet, attributable to disparities in both the length of the tail section and inlet configuration. Furthermore, it is observed that the intake process at the inlet is not synchronous with the exhaust process at the tail section.

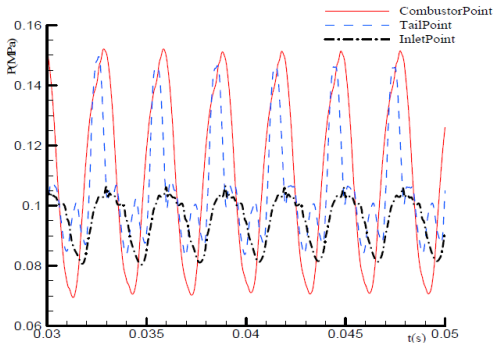

Figure 2.10-Pressure Variations (Adapted from [10]).

In conclusion, in one cycle of the pulse combustion, key parameters change alternatively in the inlet and the outlet, which is in match for the whole cycle.

To better understand the influence of admission layout on the performance of the pulsejet Geng et al. [11] performed a numerical and experimental study. To do so, they used an 8 cm hydrogen-powered pulsejet, without valves, with two inlet configurations: forward-facing and backward-facing, as sown in Figure 2.11.

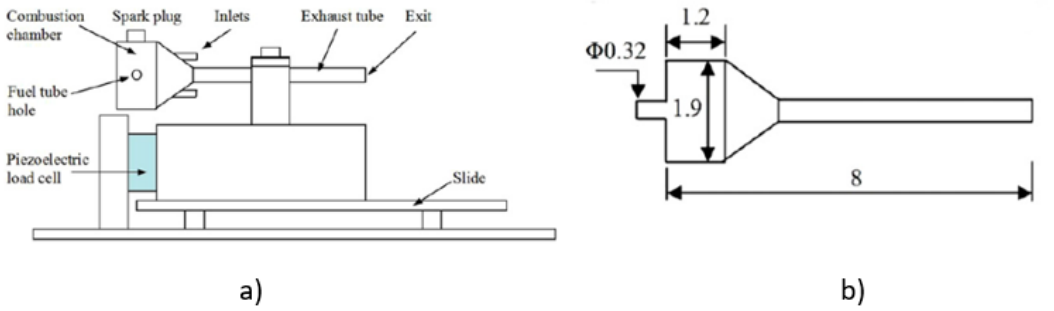

Figure 2.11- 8 cm pulsejet with a rearward-facing inlet (a) and forward-facing inlet (b) [11].

As expected, the forward-facing configuration generated very little net thrust because hot products are expelled through both the inlet and exhaust duct. With the configuration rearward-facing, an increase of approximately 1 N was achieved in relation to the configuration forward-facing.

In a low regime of fuel mass flow, the frequency and pressure exhibit a decrease and correspondingly rise as the flow of fuel increases. When the intake is forward-facing, both frequency and pressure reach their peak values in response to an increase in fuel flow. In contrast, when the intake is rearward-facing, the frequency progressively rises with the mass flow rate, while the pressure achieves its maximum at lower levels of fuel flow before reaching a stable state.

McCalley [12] conducted a study focusing on liquid fuel implementation within pulsejet engines, examining various injectors. Utilizing a twenty-five-centimenter valveless pulsejet for experimentation, the study revealed that an oversized hole in the injector restricts functionality solely to forced air operation. This is because the hole has to be small enough to create a pressure drop and force fuel out of the other holes. It has been found that if the injector has too many openings there is not enough pressure drop. Notably, an asymmetrical configuration of the holes produced a swirl effect inside the combustion chamber, which allows a quick mixing of the air with the fuel, resulting in a more homogeneous mixture. Figure 2.12 depict one of the injectors employed in these experimental assessments.

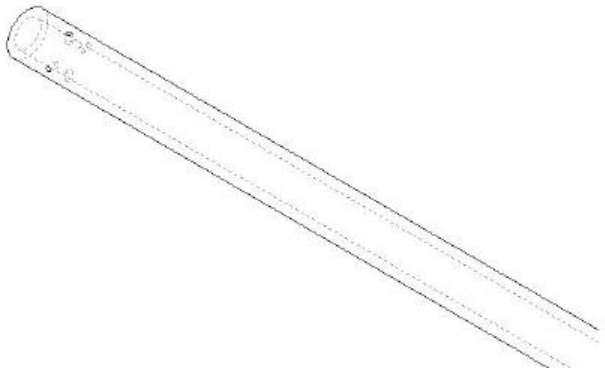

Figure 2.12- 4-hole Radial Spray Injector [12].

They verified that the jet only operated if the holes made a thirty-degree angle to a ninety-degree angle with the axis of the jet. However, the optimal orientation is still an open question. New tests were carried out to solve this problem, however, it was concluded that the drilling orientation depends on the number and diameter of the holes.

Significantly, this study underscored the challenge of initializing a liquid fuel pulsejet. Its initiation necessitates the use of propane to attain operational temperatures. Following the incandescence of the jet, propane supply ceases, and the introduction of liquid fuel ensues. This process demands more time and necessitates preheating of the engine.

In order to better understand the performance of a pulsejet Isac et al. [13] performed a numerical simulation and compared it with practice. For this, they studied the effect of the presence of flare on intake and exhaust. The simulation was started at low pressure, high temperature, and a stoichiometric mixture of propane-oxygen inside the combustion chamber, to reduce the time needed to reach the pulsating effect.
After the tests, the authors verified that the presence of a flare significantly improved the operation of the pulsejet. For the same fuel flow rate, a higher chamber peak pressure

was noticed. These components, too, helped to start the pulsing action much quicker than when a flare was not used.

Anand et al. [14] explored diverse geometries to grasp valved pulsejet mechanics, focusing on identifying compression ignition. They attributed rapid combustion to multiple synchronized auto-ignitions. Their analysis of high-resolution photos and $x - t$ combustion fluid dynamics, in Figure 2.13, allowed testing stable and unstable modes. In unstable operation, they categorized two modes: "complete failure" and "sustained instability". The first one with involves erratic bursts of fewer than ten cycles, characterized by unpredictable fill patterns, rapid combustion, and variable product expulsion speeds. The latter operates continuously until manual fuel shutdown, exhibiting instability like the first mode. Excessive fuel injection velocity led to downstream fuel movement, causing process failure, while low velocity resulted in turbulent deflagration. Ultimately, they concluded that pulsejet's rapid combustion stems from delayed auto-ignitions, allowing unstable yet sustained operation.

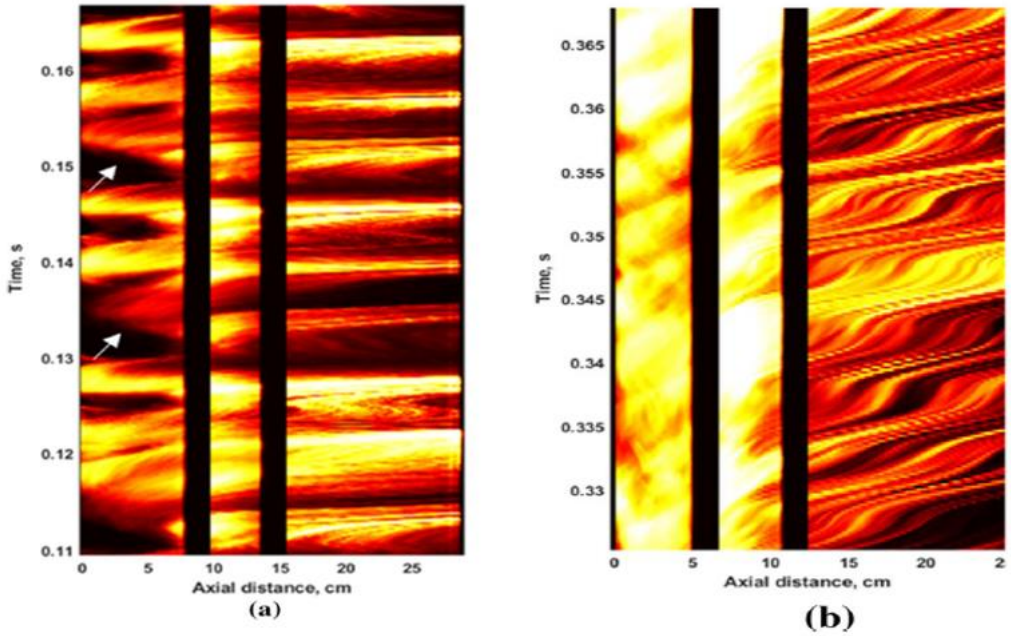

Figure 2.13-x–t plots showing (a) sustained instability and (b) complete failure, during pulsejet operation (Adapted from [14]).

Chapter 3

In order to obtain the proper functioning and performance of a pulsejet engine, it is crucial to acquire some concepts. For this, this chapter will approach the theory behind the operation of a pulsejet, thermodynamic cycles, types of pulsejets, and what are the necessary conditions for the initiation of the cycle as well as the extinction of the jet.

3.Theoretical Foundations

3.1. Pulsejet

A pulsejet engine is an intermediate between a piston engine and a gas turbine. Both pulsejets and gas turbines are types of jet engines that rely on the principle of jet propulsion to generate thrust. They produce thrust by expelling high-velocity exhaust gases in the opposite direction, as well as the linear path of the mixture from intake to exhaust. On the other hand, like piston engines, pulsejets have an intermittent combustion process.

A pulsejet is a very simple jet engine, a simple form of an air-breathing engine. This engine is extremely straightforward in its mechanics, requiring only a minimal number of moving parts or even none. It comprises an air intake, a combustion chamber, and an acoustically resonant exhaust pipe. There are three types of pulsejets: with valves, without valves, and pulse detonation engine (PDE) [1].

3.2. Valved Pulsejet

The conventional pulsejets, valved pulsejet, has one moving part, the combustor intake valve. This type of engine incorporates mechanical unidirectional valves to control the flow of air and fuel (see Figure 3.1). These valves play a crucial role in regulating the intake and exhaust processes.

In the intake phase, the valve opens to allow fresh air into the combustion chamber. As the valve opens, the air is drawn into the chamber due to the pressure difference caused by the combustion process in the previous cycle. The fuel in the form of a gas or liquid form is mixed with the air in the intake and injected into the combustion chamber. When the air/fuel is ignited, these valves slam shut, thus hot gases leave through the engine's tailpipe, thus creating forward thrust [1] [15].

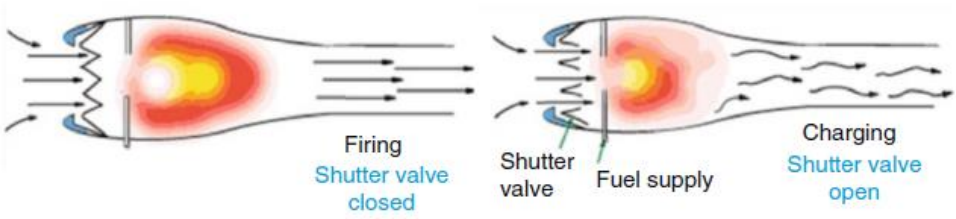

Figure 3.1- Valved Pulsejet during operation [1].

In pulsejets with valves, various types of valves can be used to control the flow of air and fuel. The choice of valve depends on factors such as the design, performance, requirements, etc. Typically, pulsejet uses reed valves, as shown in Figure 3.2. This system consists of a performed ring with drills and a petal-shaped disc that covers the same holes. These valves are located in the headwall of the main chamber.

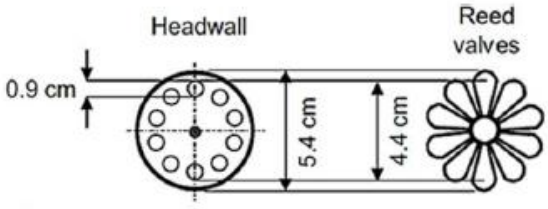

Figure 3.2- Reed Valve (Adapted from [14]).

The architecture allows a more optimized fluid dynamic of the inlet section and a larger area of openings and thus they have a smaller diameter of the combustion chamber and less aerodynamic drag [14] [16].

3.3. Valveless Pulsejet

Valveless pulsejets are a type of jet engine that operates without conventional valves. There are no moving parts and both admission and exhaustion are controlled by its geometry to control the flow of air and exhaust gases. This unique design eliminates the need for mechanical valves, simplifying the engine's structure, maintenance costs and reducing its overall weight [1].

There are several models of a valveless pulsejet, this usually depends on the accurate tuning of pressure wave passage in the applicable duct system to operate efficiently [15] They are comprised of a combustor chamber, intake duct, and exhaust duct, normally the intake tube is smaller than the exhaust tube (Figure 3.3).

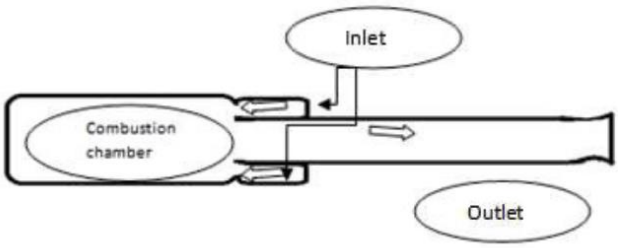

Figure 3.3- Components of valveless pulsejet engine [17].

Unlike traditional jet engines which rely on complex valve systems to regulate the flow of the air and fuel, valveless pulsejets use the rapid opening and closing of their intake and exhaust ports to create the necessary air and fuel mixture for combustion. It can be also designated as an aerodynamic valved pulsejet or acoustic-type pulsejet [1].

The engine starts using the injection of the fuel-air mixture in the combustion chamber. After the deflagration phenomenon begins, there is an increase in pressure inside the combustion chamber, as well as a compression wave, that travels through the intake and exhaust pipe [17]. When a working cycle of pulsejet is completed, the inertia of the exhaust gases induces an over-expansion, which creates a negative pressure in the combustion chamber. The cycle then repeats, with fresh air entering the engine, and is auto-ignited by remaining hot products by the last working cycle. The good performance of a valveless pulsejet depends on the dynamics of the pressure waves in the intake and exhaust [9].

3.4. Pulse Detonation Engine

Pulse detonation engines (PDEs) are an extension of pulsejet engines, they work based on the same thermodynamic cycle, Humphrey's cycle. Although there are some similarities, a PDE is a type of propulsion system that operates on the principle of detonation rather than deflagration [1].

Pulsejet operates on the deflagration of the fuel, only reaching subsonic speeds of combustion. One of the advantages of PDEs is their high thermodynamic efficiency, compared to turbines and ramjets, which use the Brayton cycle (constant pressure). The detonation process works on a constant volume combustion, which allows for more complete combustion of the fuel, resulting in better fuel efficiency compared to other engines [18].

The engine consists of a combustion chamber, usually a cylindrical tube, where the fuel and oxidizer mixture are injected (see Figure 3.4). This mixture is then ignited by an ignition source. Some studies revealed that detonation velocity is independent of the ignition source and tube diameter and is primarily a function of the explosive mixture composition [2].

After the ignition, the detonation is initiated in a tube that serves as the combustor. As the detonation wave moves through the combustion chamber, the pressure and temperature increase. The mechanism of detonation propagation is an adiabatic compression of the explosive mixture [1]. Through these intermittent detonation waves, these engines, generate thrust.

PDEs are light, easy to manufacture, reduce fuel consumption, and have the capability of operating from zero approach stream velocity to high supersonic flight speed. PDEs also have the potential for high specific impulse, which is a measure of the engine's efficiency in generating thrust [2].

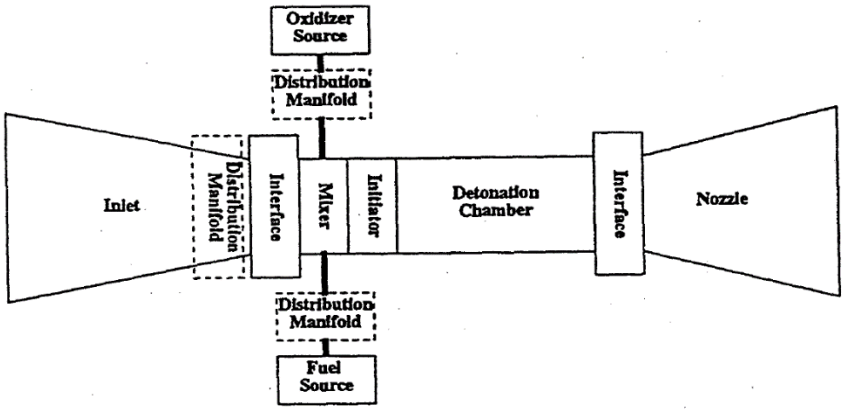

Figure 3.4- Conceptual pulse detonation engine (PDE) schematic [18].

However, the substantial noise levels and the decrease in efficiency at high Mach numbers impose restrictions on their widespread implementation.

3.5. Operational Cycle

The operation of valveless pulsejets relies on the interaction of shock waves and resonant acoustic waves within its combustion chamber to achieve combustion and thrust.

Typically, to initiate the operation of the engine and achieve self-sustained pulsations, a small quantity of pressurized air is introduced into the inlet at an inclined angle, simultaneously with the injection of gaseous fuel [19].

The operational cycle of a valveless pulsejet, as seen in Figure 3.5, can be divided into four steps: ignition and combustion, exhaust, inflow, and pre-combustion [15].

1. The combustion process initiates when the pressure inside the combustion chamber rises above atmospheric pressure. At the same time, the temperature of the fuel/air mixture increases as it combines with the remaining residual products until it reaches the temperature at which it can spontaneously ignite, known as the auto-ignition temperature [11]. The negative velocity of the cold backflow air reaches the maximum. Air continues entering the combustion chamber through the inlet but with reduced velocity.
2. During the operational cycle, compression waves are produced, causing the temperature and pressure inside the combustion chamber to rise. As a result, the flow of gases within the chamber is propelled towards both the exit and inlet, gradually gaining speed. Due to the intake duct being shorter in relation to the exhaust duct, the gases take less time to be expelled. So, expansion waves are generated at the inlet and decrease pressure in the combustion chamber. A positive velocity at the exit is increasing while the hot products flow out at the inlet with an increasing negative velocity. The pressure within the combustion chamber continues to decline, and simultaneously the velocity of the gases exiting through the inlet and exit ducts reaches its maximum. [10].
3. In the third phase of the operational cycle, the expansion wave causes the pressure within both the exhaust and the combustion chamber to drop below atmospheric levels. Consequently, the outgoing velocity at the inlet begins to diminish. This decrease in pressure leads to a reverse flow of gases at both the inlet and the exit ports. Fresh air flows into the combustion chamber through the intake during this phase. At the same time, the hot products are still being expelled through the outlet, but their velocity is reduced compared to previous stages.
4. The remaining gases and heat transferred from the chamber walls elevate the temperature of the air-fuel mixture until it reaches the auto-ignition temperature, triggering the combustion process. This complete cycle then repeats itself in a regular pattern at fixed intervals [13]. Due to the ignition occurring at several

points, called multipoint ignition, it allows the combustion time to be reduced [6].

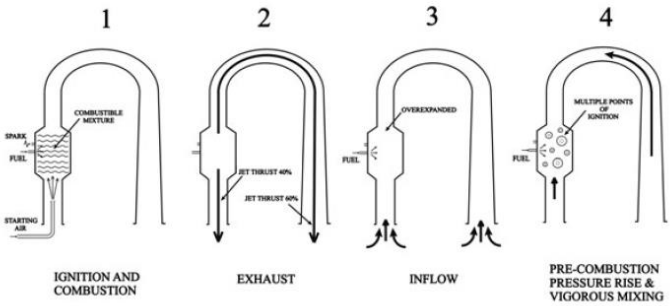

Figure 3.5-Operational Cycle of a valveless pulsejet [14].

3.6. Kadenacy Effect

There are two main models used to explain the cycle of a pulsejet engine: the Kadenacy effect and the acoustical effect. The Kadenacy emphasizes the movement of gases through pressure waves and their behaviour. This effect was initially observed by the Dutch scientist Christiaan Huygens in the 1600s, but it was named after Michael Kadenacy, a physicist who studied it in the 1930s.

As already seen, the process of combustion is responsible for elevating the temperature and pressure within the combustion chamber. When high-pressure air rapidly escapes from a rigid pressure chamber through a large opening, the pressure inside the chamber decreases to match the surrounding pressure. However, the air's inertia continues to draw air from the surrounding environment into the chamber, resulting in a decrease in the internal air pressure. Eventually, the negative pressure stops the outflow, and the reversed pressure difference draws air into the vessel to replenish it. This creates a cycle where the pressure inside the chamber fluctuates above and below the ambient pressure. The difference in pressures stops the outflow and allows the intake of fresh air into the vessel, resulting in a partial vacuum effect. As a result of the simultaneous momentum generated by the gases entering through the opposing ports, there is a momentary increase in pressure within the chamber, surpassing atmospheric levels, just before ignition takes place [4] [17].

3.7. Acoustical Theory

Another way to understand how pulsejet engines work is through the concept of acoustic resonance. It's important to highlight that both acoustic theory and the Kadenacy effect offer explanations for the operation of pulsejets, albeit with slight differences. The

Kadenacy effect elucidates pressure variations by considering flow displacement, whereas acoustic theory elucidates these variations by focusing on pressure waves.

From an acoustic perspective, a typical pulsejet engine operates on a four-pressure wave system, denoted as (C_R_R_C). This means that four sequential pressure waves, consisting of compression, rarefaction, rarefaction, and compression, propagate through the duct system (combustor and tailpipe). These waves move at or slightly above the local gas sound speed and traverse a combustion tube length of 4L within a single operational cycle [1].

In the operational cycle, the presence of acoustic resonance as the underlying cause of the pressure fluctuations can be identified. Specifically, the explosion that occurs within the chamber generates a pressure wave that interacts with the engine tube and the air enclosed within it, eliciting a resonant response. Now, due to the shape and dimensions of the combustion chamber, the returning acoustic wave can align with the natural resonant frequency of the chamber. When this alignment occurs, the pressure wave reflects back and forth between the ends of the chamber, creating a standing wave pattern.

In the graphic of Figure 3.6, the standing wave can be most accurately depicted by a double sine curve this concept also applies to the pulsejet cycle. The fluctuations of a single sine curve effectively illustrate the variations in gas pressure and gas velocity within a pulsejet engine.

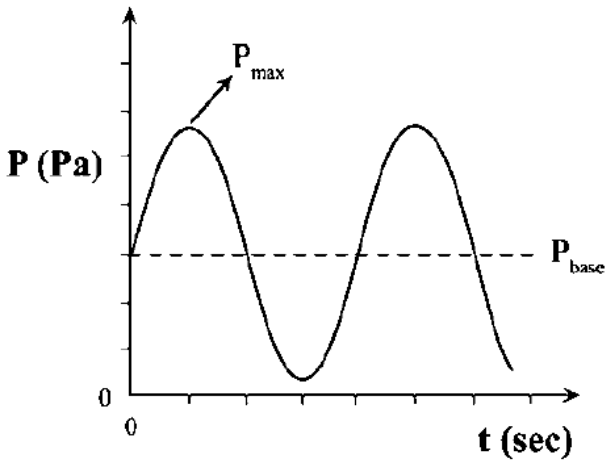

Figure 3.6-Sinusoidal fluctuations in combustion chamber pressure [1].

In acoustic terms, there are nodes and antinodes, which represent the places where velocity and pressure changes are minimal or maximum. The combustion chamber has

the highest gas flow resistance, resulting in significant pressure fluctuations. It functions as a node for velocity but an antinode for pressure. The distance between a node and an antinode determines the fundamental wavelength of the standing wave that will govern the engine operation [4].

3.8. Thermodynamic Cycle

The operation of a pulsejet can be elucidated by merging two cycles: the Lenoir Cycle, comprising continuous pressure compression, succeeded by constant volume heat addition, and adiabatic expansion, and the Humphrey Cycle, which operates similarly but includes an isentropic compression as an additional step within the cycle. The Lenoir Cycle is employed to elucidate the functioning of a pulsejet engine, while the Humphrey Cycle is utilized to describe the operation of a pulse detonation engine [5].

3.8.1. Lenoir's Cycle

The Lenoir cycle, represented in Figure 3.7, commonly employed to simulate pulsejet engines, is an idealized thermodynamic cycle inspired by Jean Joseph Etienne Lenoir's patented engine from 1860. Due to its lack of compression process, the Lenoir cycle exhibits lower thermal efficiency compared to the better-known Otto and Diesel cycles.

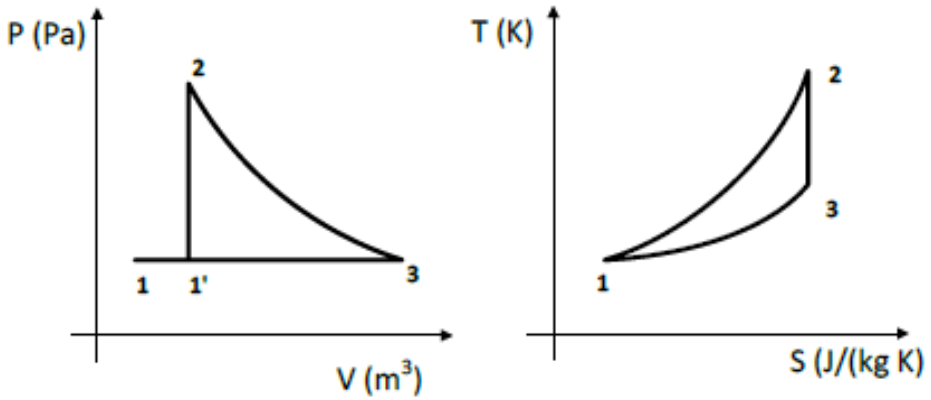

Figure 3.7-P-v and T-s for the ideal Lenoir cycle of pulsejet engine [16].

The ideal cycle comprises three stages, where:

1 → 2: Corresponds to isochoric[1] combustion.

2 → 3: Represents isentropic[2] expansion without heat exchange with the outside.

3 → 1: Corresponds to isobaric[3] heat rejection.

[1] Isochoric- Thermodynamic process at constant volume.

[2] Isentropic- Thermodynamic process with zero entropy change.

[3] Isobaric- Thermodynamic process at constant pressure.

The cycle begins with the intake of the air, represented by 3 → 1. The intake air is then compressed by the forward motion of the engine or through shock waves generated during the combustion process. Once the air is compressed, fuel is injected into the combustion chamber. Subsequently, the air-fuel mixture ignites due to heat trapped in the gases, initiating combustion within the chamber under a constant volume process. The assumption of isochoric behaviour is made as only a small number of products exit the chamber during combustion. At this stage 1 → 2, there is a substantial in pressure, temperature, and entropy. The last stage, represented by 2 → 3, involves a reversible adiabatic[4] expansion of the fluid back to its original pressure. The expanding gases leave the combustion chamber, and the pressure in the chamber drops significantly, causing a partial vacuum effect. This vacuum effect draws in fresh air for the next combustion cycle [20].

3.8.2. Humphrey's Cycle

For many authors, such as El-Sayed [1], the Humphrey cycle better explains the operation of a pulsejet, as in Figure 3.8.

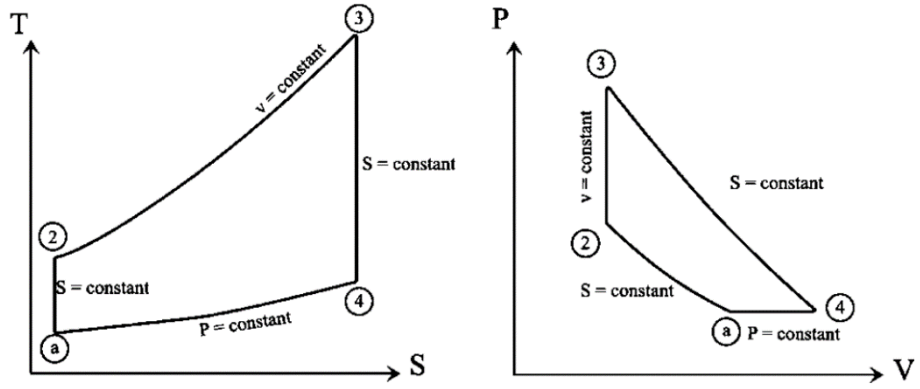

Figure 3.8- T-s and P-v for ideal Humphrey cycle of pulsejet engine (Adapted from [1]).

The Humphrey cycle comprises four stages:

- $a \rightarrow 2$: Corresponds to an isentropic compression.
- $2 \rightarrow 3$: Represents an isochoric heat addition.
- $3 \rightarrow 4$: Represents an isentropic expansion.
- $4 \rightarrow a$: Corresponds an isobaric rejection.

Subsequently, the internal thermodynamic process of the pulsejet is elucidated, along with the computation of essential parameters required to assess its performance.

- Admission Duct

[4] Adiabatic- Thermodynamic rection without heat exchange with the surroundings

This process takes place from state (a) to state (2), as illustrated in Figure 3.8. Air is drawn into the combustion chamber through. State (a) is located significantly upstream, state (1) corresponds to the pulsejet inlet, and state (2) in the same way, but on the inner side. The pressure and temperature experience an elevation from ambient conditions to the values at state (1) due to the *ram effect*[5] and these values can be determined using the provided relations:

$$P_{01} = P_{0a} = P_a \left(1 + \frac{\gamma_c - 1}{2} M^2\right)^{\frac{\gamma_c}{\gamma_c - 1}} \tag{3.1}$$

Assuming the diffuser operates as an ideal one (isentropic process), the total pressure and temperature at state (2) will be identical to those observed at state (1), or:

$$P_{02} = P_{01} \tag{3.2}$$

Nevertheless, owing to losses experienced in the diffuser, the pressure at state (2) is lower than that observed at state (1). The diffuser process is assumed to be adiabatic. Subsequently, the total pressure will be determined using a specified relation:

$$P_{02} = P_a \left(1 + \eta_d \frac{\gamma_c - 1}{2} M_a^2\right)^{\frac{\gamma_c}{\gamma_c - 1}} \tag{3.3}$$

For both isentropic and adiabatic processes, the stagnation[6] (total) temperatures at states (a), (1), and (2) are identical and can be represented by the following relation:

$$T_{02} = T_{01} = T_{0a} = T_a \left(1 + \frac{\gamma_c - 1}{2} M^2\right) \tag{3.4}$$

- Combustor Chamber

The combustion process is initiated by plug mounted atop the engine. This process takes place under conditions that closely resemble a constant-volume process. After the initial ignition, the engine sustains operation independently, with hot residual combustion gases. Consequently, for this isochoric heat addition process, the pressure ratio is as follows:

$$P_{03} = P_{02} \left(\frac{T_{03}}{T_{02}}\right) \tag{3.5}$$

[5] *Ram effect*- At high speeds, the aircraft compresses the intake air without the need for a mechanical compressor, relying on the natural aerodynamic forces instead.

[6] Stagnation temperature- is the temperature that fluid (gas or liquid) would reach if it were brought to complete stop (stagnation) and adiabatically compressed to zero velocity.

The mass flow rate of the burnt fuel is determined by analysing the energy balance of the combustion chamber:

$$(\dot{m}_a + \dot{m}_f)C_{P_h}T_{03} = \dot{m}_a C_{P_c}T_{02} + \eta_b \dot{m}_f Q_R \tag{3.6}$$

The fuel to air ratio is ascertained using the provided relation:

$$r_{c/a} = \frac{C_{P_h}T_{03} - C_{P_a}T_{02}}{\eta_b Q_R - C_{P_h}T_{03}} \tag{3.7}$$

- Tail Pipe

A consequence of the resulting high pressure and temperature, the gases are compelled to discharge from the tail at a considerable velocity. Assuming an isentropic expansion of the gases in the tail pipe towards ambient pressure, this process yields the following outcomes:

$$p_4 = p_a \tag{3.8}$$

The temperature of the exhaust gases is determined from the relation:

$$\left(\frac{T_{03}}{T_4}\right) = \left(\frac{P_{03}}{P_a}\right)^{\frac{\gamma_h - 1}{\gamma_h}} \tag{3.9}$$

The exhaust velocity is now calculated from the relation:

$$U_e = \sqrt{2C_{P_h}T_{03}\left[1 - \left({}^{P_a}/_{P_{03}}\right)^{\frac{\gamma_h - 1}{\gamma_h}}\right]} \tag{3.10}$$

The thrust force is subsequently computed using the provided relation:

$$F = m_a\left[\left(1 + \frac{\dot{m}_f}{\dot{m}_a}\right)U_e - U\right] \tag{3.11}$$

The thrust specific fuel consumption (TSFC) is given by the relation:

$$TSFC = \frac{\dot{m}_f}{T} \tag{3.12}$$

3.9. Frequency of Operation

In pulsejet engines, the operational frequency constitutes a significant characteristic. The viewpoint of scholars on this aspect remains divided, owing to the existence of various models used to forecast the operational frequency. Even so, it is worth nothing that pulsejet engines can be fabricated in diverse dimensions, rendering these formulas, not inherently erroneous.

Nonetheless, a consensus exists in one observation: the frequency of the pulsejet, whether valved or valveless, exhibits an inverse proportionality with its overall length.

$$f \propto \frac{1}{L} \tag{3.13}$$

As elucidated by the acoustic theory outlined in section 3.7, the operational frequency for a typical pulsejet is correlated with the comprehensive length of the pulsejet, which can be effectively conceptualized akin to an acoustic 1/4 wave, with a pressure node at the exhaust and a pressure antinode in combustion chamber. According to this theory, regarding a valved pulsejet, the operational frequency for one cycle is approximately [1]:

$$f = \frac{1}{\Delta t_{ciclo}} \approx \frac{1}{\frac{\lambda}{c}} \approx \frac{c}{4L} \tag{3.14}$$

Since a valveless pulsejet is essentially a tube open at both ends, it cannot be considered as a quarter-wave resonator. Typically, it features a pressure node in the center and a node at each end. According to an investigation carried out by Zheng et al. [21], valveless pulsejets, recommend the calculation of the frequency through the conceptualization of the intake as a Helmholtz resonator[7], coupled with the application of the 1/6 wave acoustic theory to simulate the characteristics of the exhaust duct.

$$f_e = \frac{c_e}{6L_e} \tag{3.15}$$

The frequency in the admission is obtained through the following equation:

$$f_a = \frac{c_a}{2\pi}\sqrt{\frac{S_a}{V_{cc}L_a}} \tag{3.16}$$

Lastly, the operational frequency of the valveless pulsejet is determined as the mean value between the previously computed frequencies:

$$f = \frac{f_a + f_e}{2} \tag{3.17}$$

[7] Helmoholz Resonator- The resonator is an enclosed volume of air communicating with the outside through a small opening. The enclosed air resonates at a single frequency that depends on the volume of the vessel and the geometry of its opening.

3.10. Maximum Static Thrust

Thrust is a mechanical force resulting from the acceleration of a gas mass, is a key parameter in jet engines, as explained by Newton's law of motion. It is a vector force determined by its magnitude, direction, and orientation, essential for propelling an aircraft forward without initial motion. section 3.8 outlines a theorical approach to calculate flight thrust in pulsejets, but practical challenges arise due to the need for escape velocity and precise fuel-to-air ratios.

In a study conducted by Tharratt [22], it was demonstrated that the maximum static thrust of a pulsejet can be predicted based solely on geometry data, independent of thermodynamics or internal engine dynamics knowledge. This is achieved Through a specific equation based on engine volume-to-length ratio.

Tharratt's equation, designed for mechanically valved ducts, remains the only method for estimating thrust in valveless pulsejets, as there are no existing studies on this topic.

$$\frac{V}{L} = 6{,}550 \times 10^{-5} \left|\vec{F}\right| \tag{3.18}$$

3.11. Starting a Pulsejet

Starting a valveless pulsejet engine can be a bit challenging, as these engines don't have traditional mechanical valves for controlling the flow of air and fuel. Instead, they rely on the dynamics of the combustion process to create a pulsating flow of gases. Three elements are required to be supplied in the correct proportion and timing to initiate its operation:

- Suitable fuel (propane, gasoline, kerosene, etc.).
- Ignition source (spark plug).
- Air compressor (for initial air supply).

In the context of practical implementation, it is recommended to initiate the process by engaging the ignition mechanism, subsequently initiating fuel, and ultimately introducing compressed air into the confines of the propulsion system [23].

3.11.1. Fuels

One notable benefit of pulsejet lies in its adaptability to operate, theoretically, with a wide array of combustible liquids or gases. It is worth noting that pulsejets are not exclusively

reliant on either liquid o gaseous fuels. Instances have arisen where coal dust was employed as a viable alternative fuel source [5].

The selection of fuel may be subject to influence by a multitude of factors, encompassing considerations such as cost, facilitation of cold initiation, as well as the dimensions and configuration of the pulsejet device.

For small pulsejet engines, is commonly used liquid propellant, such as:

- **Gasoline:** The most common fuel for valveless pulsejets is gasoline, due to its availability, energy, density and ease of combustion.
- **Kerosene:** Kerosene is used for larger pulsejets or those designed for specific applications. The challenge associated with this variety of propellant pertains to the intricacy of initiating the combustion without high pressures.
- **Hydrogen (H_2):** In certain experimental setups, such as Geng et al. [11], hydrogen gas can be used as fuel for valveless pulsejets. Hydrogen has a high energy content and burns cleanly, producing only water vapor as a byproduct. However, hydrogen's low energy density and challenges associated with storage handling make it less common.
- **Alcohol-based fuels:** Some valveless pulsejets can be operated with alcohol-based fuels, the most common is methanol (CH_3OH). These fuels can burn more cleanly and produce less soot compared to hydrocarbon fuels like gasoline. Methanol exhibits appealing attributes owing to its elevated calorific potency; however, the high flammability index and invisible flame during the burning make its handling dangerous.

Beyond liquid fuels, combustible volatile gases, such as butane (C_4H_{10}), methane (CH_4), and propane (C_3H_8), can also serve as fuel sources for the combustion process, the distinct advantage of utilizing gaseous fuels in contrast to their liquid counterparts lies in the absence of a requisite fuel pump. Instead, pressurized introduction of gas into the reservoir serves a dual purpose by simultaneously fulfilling the role of a pressurization mechanism. Furthermore, the substantially lower boiling points of these gases in comparison to ambient temperatures obviate the need for vaporization, a requirement inherent to liquid fuels. The regulation of gas flow directly into the combustion chamber

can be governed through the utilization of regulator positioned at the outlet nozzle of the tank.

3.11.2. Air Supply

To start a valveless pulsejet engine involves creating the initial conditions necessary for combustion to initiate and sustain within the engine's combustion chamber. An external force such as a manual air blower, compressed air, or an electric starter motor can be used to provide the initial airflow required for combustion.

If the prolonged air source is removed or air pressure remains insufficient, combustion would proceed with an excessively rich mixture. This results in the ejection of a string flame through the propulsive nozzle, while the distinctive pulsating phenomenon would not occur.

Once the engine reaches its self-sustaining operating conditions, it continues to cycle on its own if the proper fuel-air mixture and ignition are maintained [23].

3.11.3. Source of Ignition

To start a valveless pulsejet, an ignition source is needed to initiate combustion. Some common ignition sources used for starting valveless pulsejets include:

- **Spark Plugs:** The best ignition source is a spark plug mounted in a combustion zone section of the engine. A spark is generated across the spark plug's electrodes, which ignites the fuel-air mixture.
- **Glow Plugs:** Glow plugs are like spark plugs but rely on the heating of a wire filament to ignite the fuel-air mixture.
- **Torch Igniters:** Torch igniters produce a continuous flame that can be directed into the combustion chamber to initiate ignition. This flame heats up the mixture until it starts to combust on its own.
- **External Flame:** An external flame source, such as a blowtorch or a pre-existing flame, can be used to ignite the fuel-air mixture.

The ignition source functions akin to the introduction of pressurized air solely during the engine initiation phase, rendering its presence superfluous upon attainment of consistent operational conditions. Subsequent cycles of the thermodynamic process are sustained through the utilization of residual combustion gases [23].

Chapter 4

4.Experimental installation

Within this chapter, a comprehensive exposition will be provided, including the entirety of the pulsejet's developmental progression. Initial deliberations and blueprints will be expounded upon, alongside an elucidation of the materials used and the manufacturing processes employed. Furthermore, the three systems complementary to the operation of the pulsejet will be specified.

4.1. Inicial Pulsejet SetUp

The precise geometry of pulsejet components is indispensable for achieving the desired resonance, combustion efficiency, and overall performance of these engines. It directly influences their capacity to generate thrust efficiently and sustain pulsating combustion, making it critical for their successful operation [19].

The working of pulsejets is still not well understood and hence most of the designs are still made on an empirical basis. Based on research carried out at UBI [6], [24], [25], it became feasible to establish a geometric correlation among all the constituent elements of the pulsejet (see Figure 4.1). Therefore, the investigation focuses its attention on the development of Chinese design valveless pulsejet, characterized by the ensuing geometric parameters:

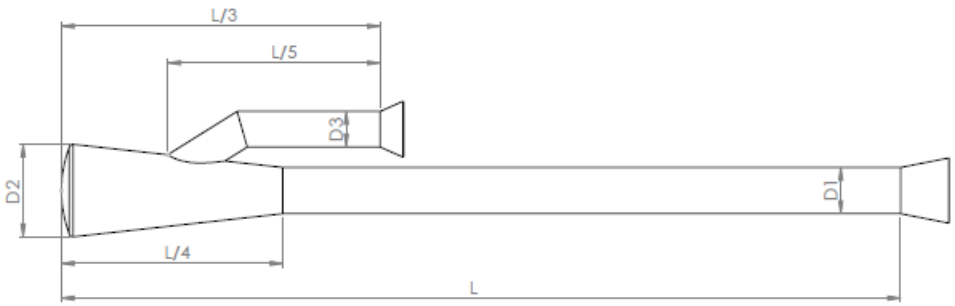

Figure 4.1- Pulsejet dimensional configurations.

Kowing that:

$$L = 12{,}1D_m \tag{4.1}$$

$$D_m = \frac{D_1 + D_2}{2} \tag{4.2}$$

$$D_m = \frac{D_3 + D_1}{2} \tag{4.3}$$

$$D_1 = \frac{D_2}{2} \tag{4.4}$$

$$D_3 = \frac{D_1}{1{,}3} \tag{4.5}$$

Taking into account dimensional constraints and product accessibility within the market, the sizing of the pulsejet was conducted, ultimately resulting in the formulation of the initial project through the utilization of the CAD software, SolidWorks, as illustrated in Figure 4.2.

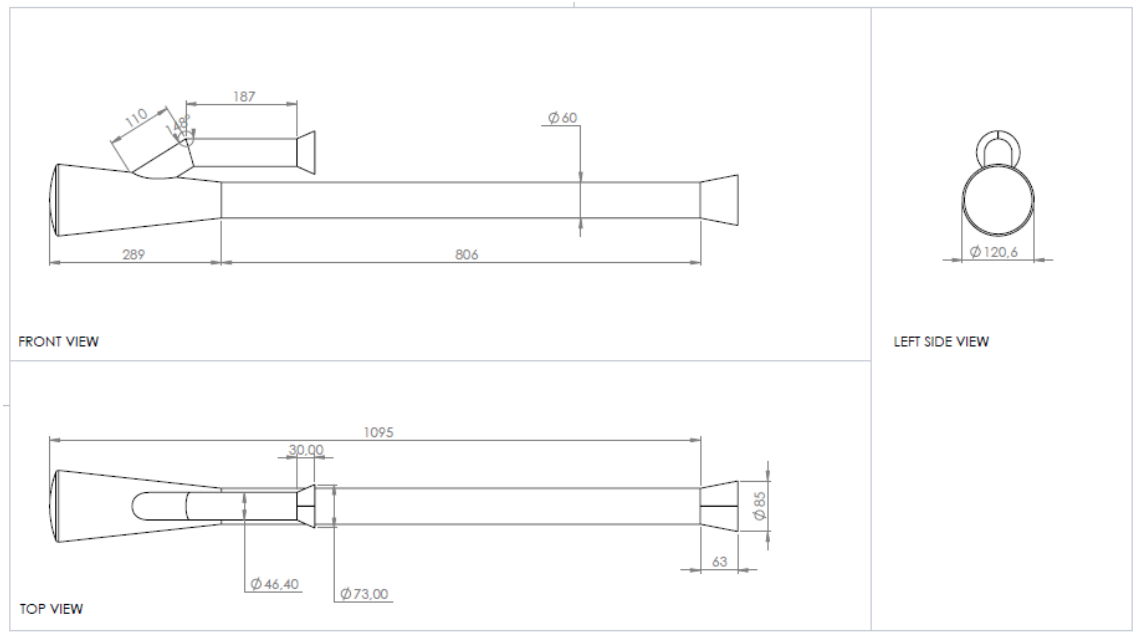

Figure 4.2- The three main views of the initial project.

4.2. Manufature of the Pulsejet

To ensure optimal performance and achieve favourable outcomes across various testing scenarios, the process of material selection for pulsejet engines involves a careful balance between performance and durability. When choosing materials for pulsejet engines, the material must be resistance to high temperatures, resistance to corrosion, affordable price-quality and available on the market considering the project dimensions (see Table 4.1). To safeguard the operational integrity of the pulsejet during the tests, steel materials with a thickness of 2 mm were employed.

The most suitable material that fulfils all the aforementioned requirements is stainless steel 1.4835, supplied by the company *Inaceinox, SA*.

Stainless steel 1.4845 was applied to the intake pipe, but its selection and justification for choosing it as an alternative steel will be explained in subsequent sections.

Table 4.1- Properties of steel 1.4835 and steel 1.4845 [26].

Stainless Steel	EN 1.4835	EN 1.4845	Units
Mechanical Properties			
Brinell Hardness	180	170 to 210	-
Elastic Modulus	200	200	GPa
Elongation at Break	43	34 to 44	%
Fatigue Strength	310	250 to 280	MPa
Poisson's Ratio	0.28	0.27	-
Shear Modulus	77	79	GPa
Shear Strength	520	420 to 470	MPa
Thermal Properties			
Maximum Temperature: Corrosion	703	723	K
Maximum Temperature: Mechanical	1423	1373	K
Specific Heat Capacity	490	480	J/kg-K
Thermal Conductivity	15	16	W/m-K
Thermal Expansion	17	16	$\mu m/m - K$
Otherwise Unclassified Properties			
Density	7700	7900	kg/m^3

All manufacturing and assembly processes were conducted at *Inaceinox, SA*, and will be explained in the following sections.

4.2.1. Admission

Given the initial project dimensions and the tubing options available in the market, the selection was made to use stainless steel 1.4845 for fabricating the inlet component (see Figure 4.3). Nevertheless, the tubing readily accessible in the market possessed dimensions Ø48.26×3.68 mm. To conform to the precise specifications of the project, the tubing underwent extensive external and internal turning procedures.

Subsequently, for accommodating the requisite 148° bend in the inlet, the angle was accurately determined using a horizontal ribbon saw. Finally, the assembly of the two components was accomplished through the application of a TIG (Tungsten Inert Gas) welding bead.

Figure 4.3- Admission.

4.2.2. Combustion Chamber

For the combustion chamber and the remaining components, a sheet of 1.4835 steel measuring 2.00×1500×6000 mm was employed. Flattening has become easier with the use of SolidWorks, as demonstrated in the Appendix B. Consequently, to achieve the desired geometry, the combustion chamber was delineated onto the sheet, followed by its cutting through a plasma cutting process and subsequent grinding using an electric grinder.

Subsequently, through a plastic forming technique known as calendaring, the sheet was manipulated to attain the required shape. However, following this procedure, the combustion chamber's diameter deviated from the desired specifications due to its diminutive dimensions. To rectify this, a hydraulic press, as illustrated in Figure 4.4, was utilized, resulting in the attainment of the intended perfect diameter.

Figure 4.4-Press to give the final shape to the Combustion Chamber.

Ultimately, a TIG welding process of full penetration was executed, wherein the groove of the base material intended for joining was fused and integrated with the molten filler material (see Figure 4.5).

Figure 4.5- TIG Full Penetration Welding in the Combustion Chamber.

The top assumes a domed configuration a slight curvature, due to the high pressures inside the combustion chamber, so that it does not cause any deformation in the engine. To manufacture the domed top, a cold pressing technique was employed, using a die and punch arrangement to achieve the desired geometric shape (see Figure 4.6).

Figure 4.6- Domed Top.

4.2.3. Exhaust

The manufacturing procedure for the exhaust system was similar to the combustion chamber. Nevertheless, due to the length of the tube, it necessitated being partitioned into two segments, given the unavailability of a suitable calender for the project's dimensions. Thus, these two segments were united through a circular TIG welding seam (see Figure 4.7).

Owing to the presence of a discontinuity within the welding region, flow disturbances occur, resulting in elevated temperatures within the affected material. Consequently, this leads to a reduction in the engine's thrust output. To mitigate this issue, the welds were intentionally grinded from the interior, without causing any damage, utilizing a lamella for assistance.

Figure 4.7- TIG Full Penetration Welding in the Exhaust.

4.2.4. Flares

In accordance with findings by Isac et al. [13] the incorporation of a flares has been shown to enhance the operational efficiency and frequency of a pulsejet engine. This assertion is corroborated by the research conducted by McCalley [12], wherein the inclusion of flares facilitated the ignition process of the pulsejet engine. The underlying rationale for this phenomenon lies the context of pulsed combustion, wherein vortices are generated at the interface between the exhaust and the surrounding atmosphere. By introducing a greater pressure differential at the outlet of the exhaust pipe, the partial vacuum within the combustion chamber, responsible for air intake, undergoes augmentation, thereby contributing to the self-sustaining mechanism of the engine.

The manufacturing process of flares closely resembles that of the combustion chamber. In the Appendix B.2 and B.3, can observe the geometrical characteristics of the intake and exhaust flares, respectively.

4.3. Test Bench

The test bench used in the course of this project was designed and built by a former UBI student [6]. Despite this, the configuration and arrangement of the bench are described below, as can be seen in the Figure 4.8.

The construction of the test bench involved the use of steel profile components with a square cross-section measuring 16×16 mm. This structure ensures the stability of the pulsejet during the static tests and withstand the considerable vibrations associated with this type of propulsion system.

For precise measurement of the engine's traction force, two rails with bearings were integrated into the bench to directly transmit this force to a load cell. Furthermore, a carriage was positioned above these sliding rails, designated not only to support the engine's weight but also to move it away from the rails when necessary. Given the substantial thermal energy generated by the thruster, which could potentially compromise the integrity of the plastic bearings in the rails, the pulsejet was raised by 18 cm to enhanced heat dissipation into the surrounding environment. This adjustment guaranteed a dependable traction measurement transmitted to the load cell via steel cable.

The test bench's structure was secured to a worktable using three pressure clamps, facilitating easy transportation and potential relocation of the bench without the need for permanent attachment.

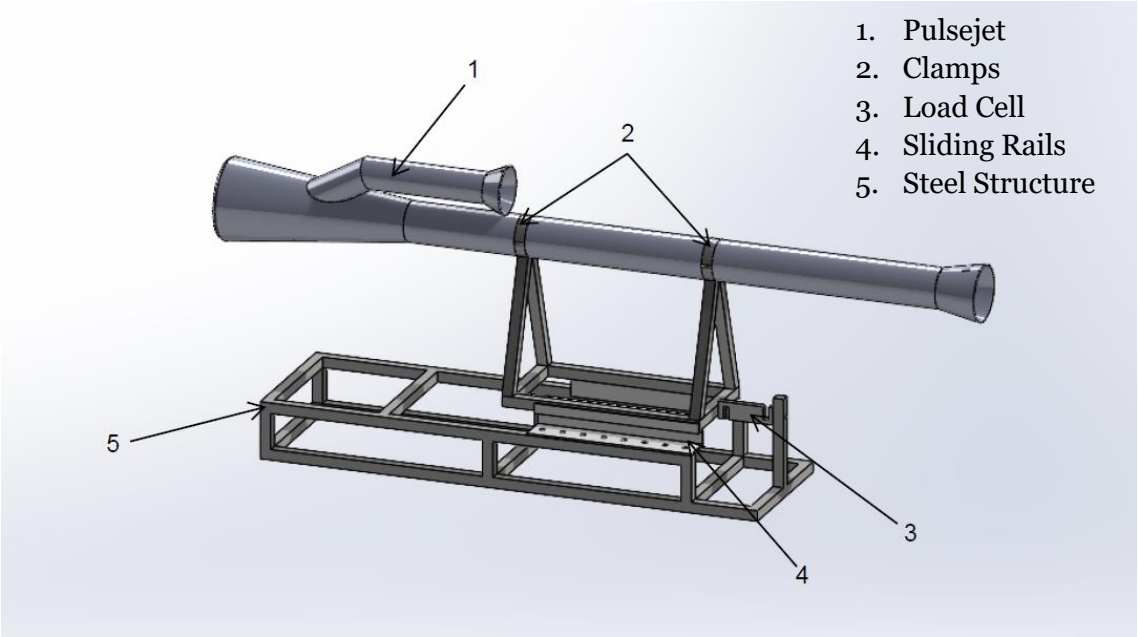

Figure 4.8- SolidWorks drawing of the Pulsejet installed on the Workbench.

4.4. Fuel

Pulsejets are renowned for their adaptability in fuel selection. The primary goal of this thesis is to develop a pulsejet engine that runs on liquid fuel. This task presents a significant challenge in the fuel delivery process because gaseous fuels like propane are already vaporized, eliminating the need for atomization or complex injection systems.

For this project, an atomization process was used, testing various spray nozzles. This approach was chosen for its simplicity, the ease of acquiring material, and its cost-effectiveness. The components that make up the injection system will be properly explained in section 4.5.2., including their arrangement within the system.

Pulsejets have the capability to operate using gasoline, diesel fuel, and kerosene. Among these options, gasoline is generally considered a superior choice for pulsejets. This preference is due to its relatively narrow flammability range, which means it will flame out (blow out) if the fuel-air mixture is too lean or too reach in the combustor. This unique characteristic enhances the pulsejet's ability for intermittent burning, as opposed to continuous burning [15]. Gasoline with a 95-octane rating was chosen for its volatility which eases the atomization process.

4.5. Complementary Systems

4.5.1. Ignition System

The ignition system in a pulsejet engine is responsible for creating a high-voltage spark to ignite the air-fuel mixture within the engine's combustion chamber. This ignition process is crucial for the engine to start and operate continuously in a pulsating manner. The spark plug, identified as an NGK CMR6H model, is strategically placed on the wall of the combustion chamber's domed top, with an M10× 1 mm thread skilfully carved into the chamber's wall to secure it in place, as shown in Figure 4.9.

In order to initiate the electrical discharge, an ignition module rated at 20 kV and a discharge frequency of 16 Hz was acquired. This module is powered by a 3-cell lithium polymer battery with capacity if 11.1 V and 2100 mAh.

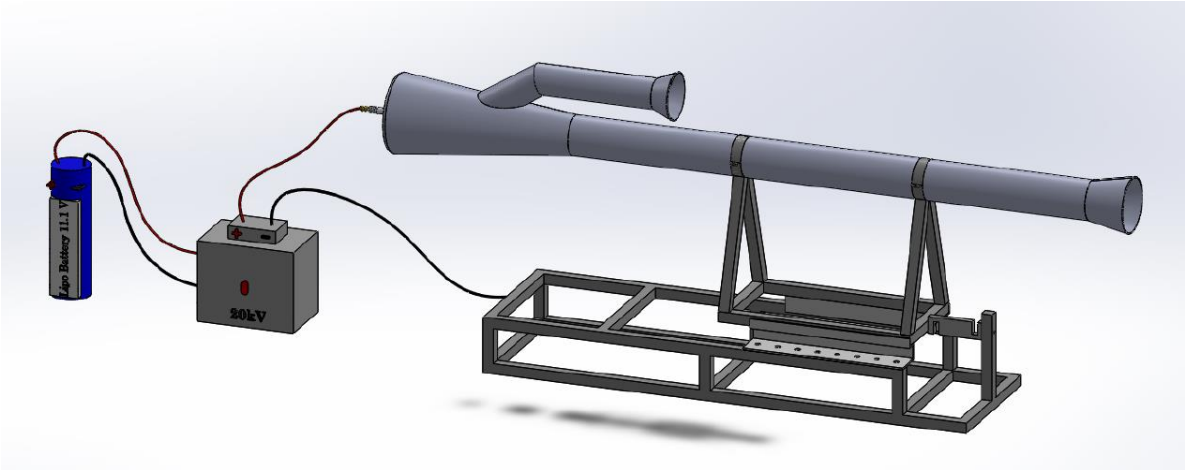

Figure 4.9- Ignition System.

Upon activation of the ignition module, there is a passage of 20 kV of current through the positive terminal, reaching the spark plug. This results on generation of intermittent high-frequency sparks. Meanwhile, the negative terminal, which is connected to the common ground (in this context, the test bench), is responsible for absorbing the entirety of the electrical load. It is important to note that while the actual direction of electric current is from the negative to the positive pole, this description adheres to the conventional direction to current flow. Once the Pulsejet attains self-sustainability, the ignition system is subsequently deactivated.

4.5.2. Fuel Injection System

In the utilization of liquid fuel, specifically gasoline in this context, the requirement arises for an effective injection system (see Figure 4.10). As already mentioned, an atomization process was used to delivery fuel into the combustion.

Atomization refers to the process of breaking down a liquid fuel into tiny droplets or particles, increasing the surface area of the fuel. This is done using nozzles, as in the Figure 4.11. In a valveless pulsejet, proper atomization is vital as it ensures the uniform dispersion of small fuel droplets, enhancing their interaction with the surrounding air. This critical process guarantees even fuel distribution within the combustion chamber, fostering a homogeneous blend of air and fuel. This uniform mixture facilitates consistent combustion, ensuring the engine operates stably [5] [27].

Combustion instability poses a persistent challenge in the advancement of valveless pulsejet engines, where precise control over the combustion process is limited compared

to engines with valves. This results in recurrent pressure fluctuations in the combustion chamber with highly variable frequency amplitudes [28].

Therefore, designing the best injection system for a valveless pulsejet engine using gasoline involves careful consideration of various factors such as fuel atomization, mixing efficiency, combustion stability, and overall engine performance. In order to accomplish all the specified objectives, the injection system comprises a fuel tank, a fuel filter, a pump, a ball valve, a nozzle and a pressure gauge.

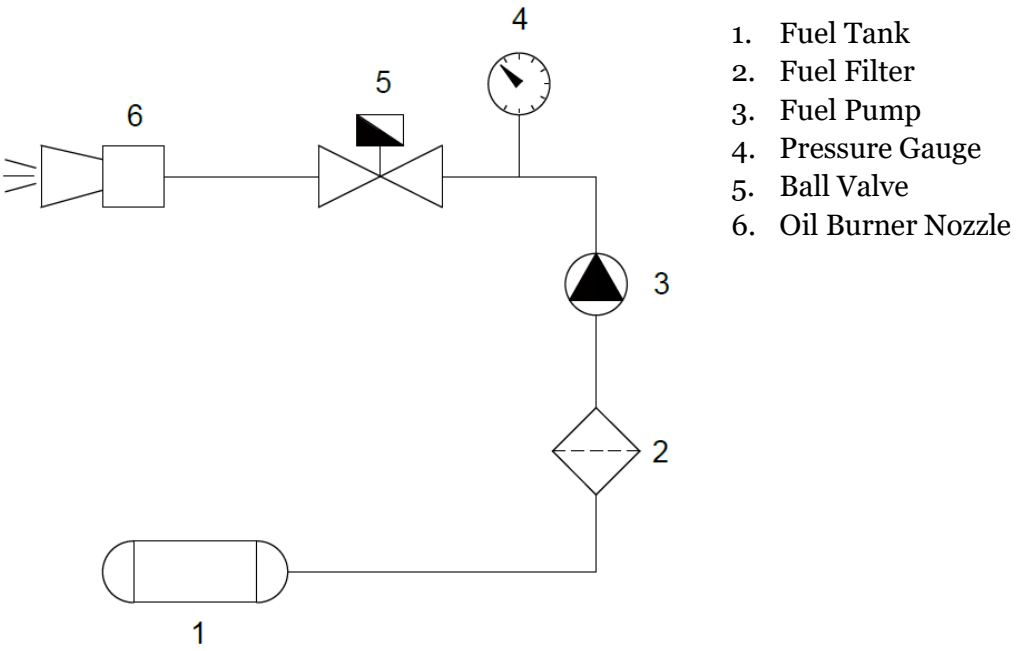

Figure 4.10- Schematic representation of the Injection System.

4.5.2.1. Fuel Filter

The primary purpose of a fuel filter is to filter out impurities and contaminants present in the gasoline before it reaches the nozzle. Gasoline can sometimes contain particles, debris, and sediments that can obstruct the fuel nozzle injector and can lead to serious damage. The gasoline filter traps these impurities, preventing them from entering the fuel injectors.

4.5.2.2. Fuel Pump

The PowerMax Universal FP1 fixed displacement pump, employed in the injection system, consistently moves a set fluid volume per cycle, irrespective of the encountered pressure. Meanwhile, the primary function of the fuel pump involves extracting fuel from the tank and raising its pressure to 10 bar. This elevated pressure aids in breaking down fuel into finer droplets, encouraging a more comprehensive and uniform mixture with

air. Specifically, the utilization of oil burner nozzles effective at 10 bar initiates the atomization process at 7 bar.

Control over spray instabilities can be achieved through liquid velocity modulation. Increasing injection pressure correlates with higher drop velocities, exerting substantial influence on the injection angle. Higher injection speeds lead to broader angles., shaping the dispersion and coverage area of resulting sprays. These factors significantly affect mixing efficiency [29].

This mechanism holds significant importance as it influences nearly all injection parameters, particularly affecting the size of fuel droplets. To calibrate the fuel injection system for optimal atomization pressure, ensuring efficient, clean, and reliable operation, preliminary tests were conducted to assess fuel dispersion patterns.

4.5.2.3. Nozzles

An oil burner nozzle is engineered to deliver a precise volume of fuel into the combustion chamber, ensuring a consistent spray pattern and angle tailored to the specific needs of a particular burner. This nozzle atomizes the fuel oil, breaking it down into minuscule droplets, facilitating rapid vaporization essential for efficient combustion.

The breakup of a liquid jet into filaments and droplets involves overcoming surface tension forces, often facilitated by centrifugal forces in a swirling liquid jet. This technique involves introducing liquid through tangential holes into a swirling chamber, generating a rotating liquid film due to centrifugal force. Concurrently, gas flows through specific channels and enhances atomization upon interacting with the liquid at the injector orifice [28].

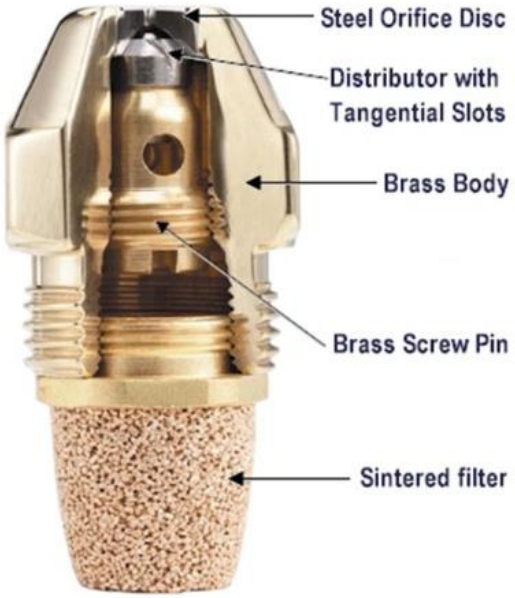

Figure 4.11- Diagram of a Fuel Nozzle Injector used in experimental tests [28].

The appropriate selection of oil burner nozzles for this injection system necessitates careful consideration of three key factors: the flow rate specific to each nozzle, the injection angle, and the spray pattern.

An experimental study by Duarte [6], using propane in a valveless pulsejet, demonstrated self-sustainability at a maximum flow rate of 7.7 g/s. Considering this and the availability of injectors on the market, tests were conducted with injectors with a maximum flow rate of 3 g/s, 3.5 g/s and 4 g/s.

The selection of this angle is determined by the requirements of the burner's air pattern and the configuration of the combustion chamber. In the contest of a Chinese-type valveless pulsejet with a long narrow combustion chamber, the recommended spray angle typically ranges from 30° to 60° (see Figure 4.12).

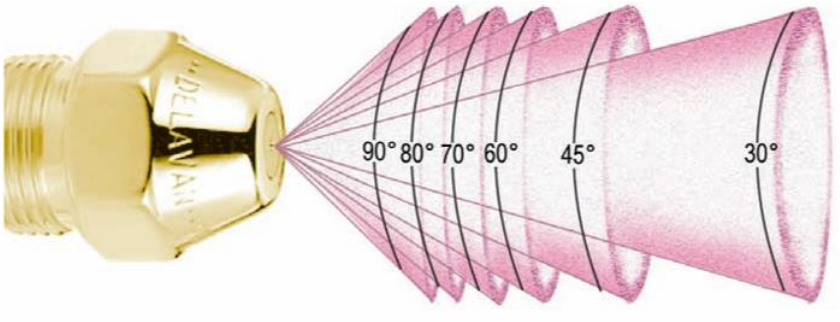

Figure 4.12- Spray angles [28].

The spray pattern and angle ensure that all droplets burn completely while suspended in the combustion area. The solid cone pattern is recommended by its even fuel droplet distribution within the cone, making it suitable for long fires(see Figure 4.13) [27].

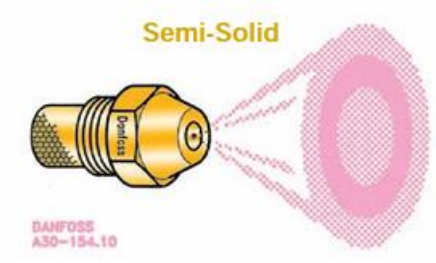

Figure 4.13- Spray pattern [28].

Taking into account the information mentioned earlier and considering market availability, the nozzles have a spray angle of 45° and feature a semi-solid (SS) pattern.

The injection system can be schematically represented by the following figure:

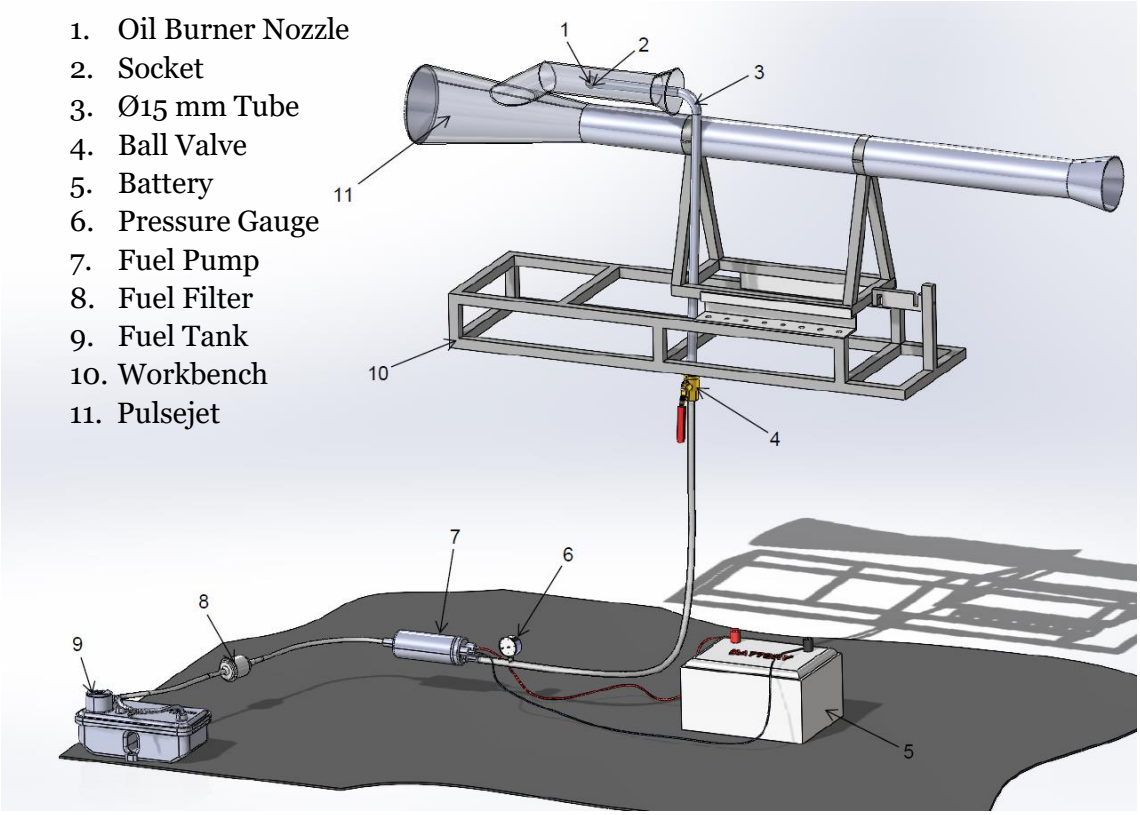

Figure 4.14- Representation of the Injection System in SolidWorks.

It is noteworthy that the system is governed by a ball valve (component 4 in the Figure 4.14) responsible for regulating the injected flow volume.

Additionally, it is observed that the oil burner nozzle is affixed to a CNC-machined socket (component 2 in the Figure 4.14) tailored to accommodate the 14× 1 mm nozzle thread, subsequently welded to a 15 mm diameter tube (component 3 in the Figure 4.14). Precision in crafting the socket was imperative to prevent pressure leaks and, consequently, to achieve optimal atomization.

4.5.3. Compressed Air System

Compressed air creates an initial pressure and help to stabilize the combustion process in a valveless pulsejet engine during startup. It can provide a consistent flow of oxygen, which is necessary for combustion to occur.

To achieve this objective, an air compressor was employed, positioned within the UBI Aeronautical Engineering Department's hangar, and linked to device designed to regulate the air pressure supplied to the engine.

Once the engine is running, it can sustain the cycle without the need for additional compressed air. This is accomplished by the intake creating a partial vacuum within the

chamber through the swift explosion of combustion byproducts, ultimately achieving the self-sustaining pulsating effect.

4.6. Operational Problems

4.6.1. Flow rate

According to Wenxiang's [9] numerical investigation, the initial tests used a nozzle supplying only 0.4 g/s of gasoline directly into the combustion chamber. However, despite changing the injector to different positions, this flow rate proved insufficient for effective fuel and air mixing in the engine being studied.

In Duarte's [6] investigation, it was determined that injecting a flow rate below 1.4 g/s of C_3H_8 significantly impedes the attainment of a self-sustaining effect without supplementary air. This finding, considering the similar geometry of the pulsejet under examination to that in Duarte's study, can be considered a valuable reference point, accounting for specific characteristics of gasoline and propane.

Considering the lower calorific value of propane at 46.4 MJ/kg and that of gasoline at 43 MJ/kg, it can be inferred that a greater flow of gasoline is required to generate an equivalent level of thrust compared to propane. Additionally, the differing stoichiometric air-fuel ratios (AFR) 14.7:1 for gasoline and 15.67:1 for propane-suggest a greater need for air during combustion with propane in the engine. Experimentally, it is impractical to regulate the air volume in the mixture. Therefore, assuming equal air intake in both scenarios, achieving similar results requires a 7% increase in gasoline flow compared to running the engine on propane.

As a result, the measurements of gasoline flow were exclusively derived from a nozzle delivering 4 g/s, with regulation managed by a ball valve. The remaining nozzles proved inadequate in delivering the required flow and were thus excluded from the experimental trials.

4.6.2. Pulverization

Initially, there was a return in the injection system, controlled by a pressure-regulating valve. However, during the tests, this setup failed to generate the required pressure for fuel atomization within the primary injection line. Therefore, direct fuel injection was chosen.

Upon the installation of the pressure gauge, it was possible to verify at what pressure the fuel was being injected. When the pump was connected, gasoline was injected at 10 bar. However, the pressure swiftly decreased to 8 bar, exhibiting fluctuations between 7 bar and 8 bar. This was due to the use of a fixed-displacement fuel pump. Such pumps encounter challenges in sustaining a consistent pressure, primarily attributed to variations in flow and the presence of system leaks.

To reduce leaks, the connections were reinforced using clamps and teflon. A slight improvement was observed; however, the system operated only at a maximum pressure of 8 bar.

4.6.3.Startup Procedures

The primary challenge faced in this project unequivocally centered around the initiation process of the gasoline pulsejet. When dealing with liquid fuels, it becomes imperative to factor in the durations required for mixing and vaporization. Consequently, it is crucial not solely for the chemical reaction rate to be swift, but also for the processes of vaporization and mixing to be executed expeditiously to enable reactions to outpace the operational frequency of the jet [12].

Following numerous trials, it was observed that the initiation and operational efficiency of the engine exhibited improvement with increased pulsejet initiation temperatures. Since it enabled vaporization and mixing to occur as expeditiously as possible. Therefore, it was necessary to use propane to elevate both the temperature of the liquid fuel and the pulsejet itself, resembling McCalley's [12] procedure in his practical test.

The engine is initially started with propane following the procedures described in section 3.11. The propane fuel injector was positioned identically to that of the liquid fuel injector. Once the pulsejet generated consistent thrust with propane, the airflow was interrupted. When the jet is incandescent, the fuel pump is turned on, allowing high-pressure gasoline to be injected in vapor form. However, this fuel injection induced instability, necessitating a subsequent adjustment of the airflow. The propane flow was reduced, and meticulous control over the airflow was implemented until the engine operated exclusively on gasoline, ensuring a constant thrust.

Once the engine reaches a heated incandescent combustion chamber, the airflow can be gradually diminished, concurrently with the deactivation of the spark plug. This process leads to the pulsejet attaining a self-sustaining state.

4.6.4.Position of the Injector

During the experimental phase, a critical inquiry emerged concerning the optimal placement of the injector. As indicated by Duarte's [6] research, the most favourable position for injection was identified to be within the midsection of the intake tube.

Nevertheless, in the context of this gasoline-focused study, initial tests commenced with the injector directly situated within the combustion chamber. This strategic placement aimed at mitigating the potential transformation of gasoline into liquid state after its atomization, a consequence attributed to the impact against the walls of the intake tube.

Despite these efforts, this approach yielded suboptimal outcomes. Numerous attempts to initiate the engine using this configuration proved futile. Consequently, a repositing of the injector to the midpoint of the intake tube, as depicted in Figure 4.15 was implemented. Remarkably, this adjustment resulted in enhanced engine performance, achieving the sought-after self-sustaining effect. The enhancement is due to injecting fuel into the intake, allowing for better atomization and thorough mixing with incoming air, vital for efficient combustion. This ignited fuel-air mixture creates the needed thrust to propel the pulsejet engine.

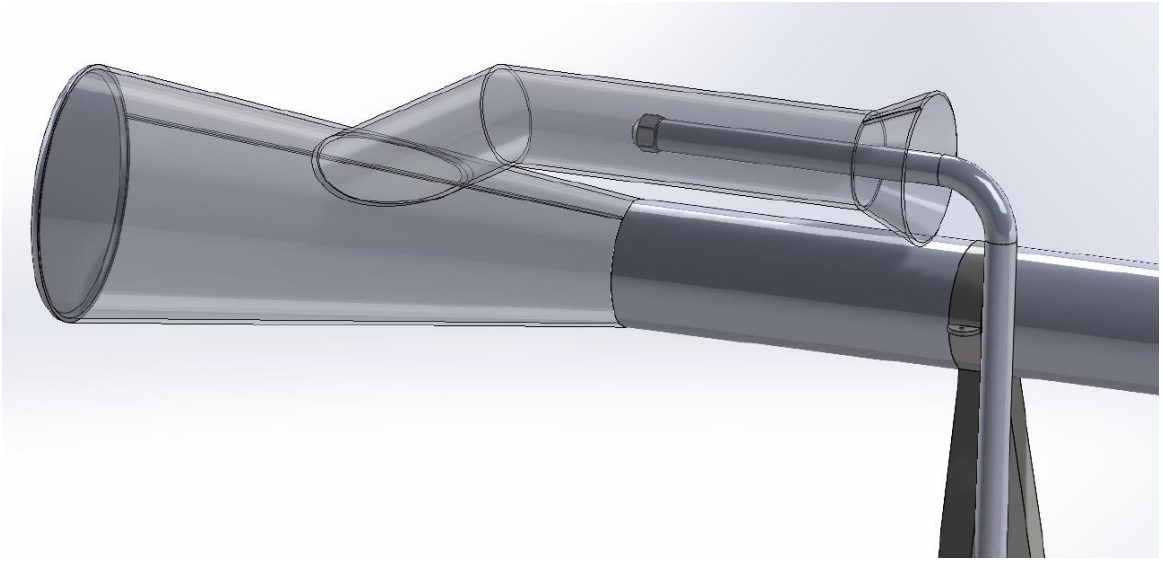

Figure 4.15- Optimal position of the oil burner nozzle in the intake duct.

Chapter 5

5. Experimental Tests and Results

This chapter aims to outline the methodology used acquire experimental data, present the findings demonstrating the engine's operation, detail the types of sensors employed with their specifications and strategic placement within the jet engine, and finally, showcase the codes instrumental in data acquisition.

5.1. Data Acquisition Instruments

To comprehensively analyze the engine's performance and gain insights into its functioning, data collection during the tests was imperative. This involved measuring the thrust, temperature, fuel consumption, and valveless pulsejet frequency. Sensors were strategically positioned to mitigate potential damage, particularly considering the elevated temperatures generated during engine operation (see Figure 5.1). The collected sensor data were transmitted to a hardware board, specifically an Arduino Mega 2560, for further processing and analysis.

5.1.1. Temperature

To determine the theoretical operational frequency of the pulsejet, as outlined in section 3.9, temperature monitoring was essential at both the intake and exhaust ducts. To achieve this, two type "K" thermocouples, possessing a thermal range from $[-260, 1260]\,°C$ were employed. These thermocouples use distinct metallic alloys, usually chromel and alumel, conjoined at one end. The other is connected to the electromotive force (EMF) measuring instrument, closing an electrical circuit through which the current flows. The MAX6675 amplifier was tasked with converting the signal originating from the thermocouple into digital form for transmission to the *hardware* board.

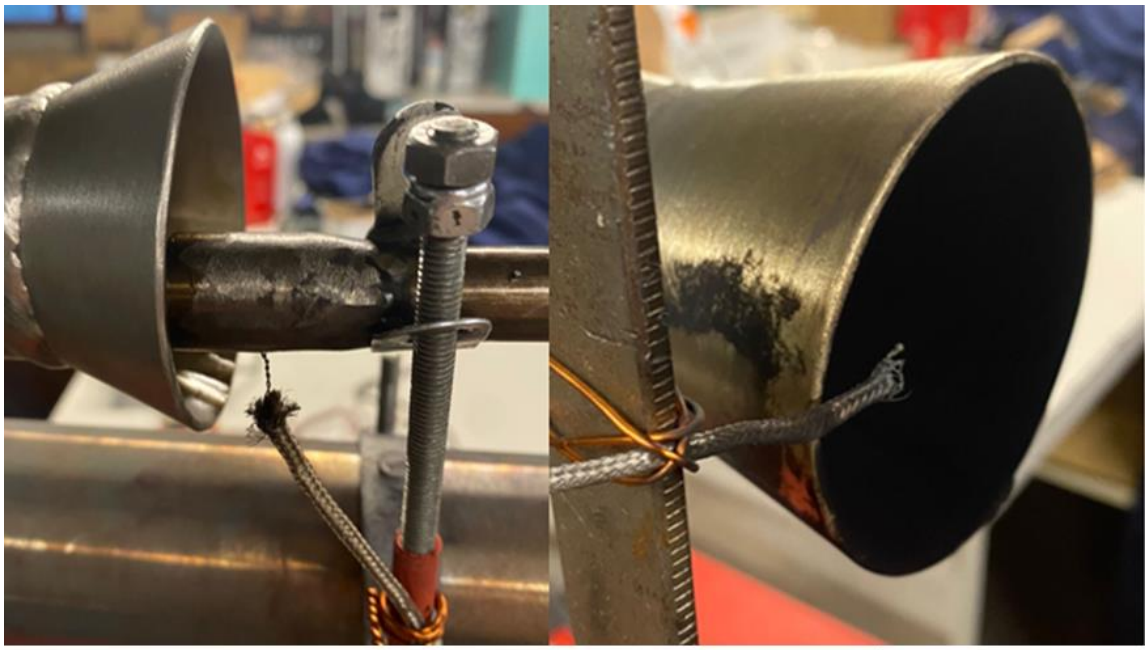

Figure 5.1-Position of Thermocouples-a) Admission; b) Exhaust.

5.1.2. Thrust

The thrust of the engine was measured using a DYLY-103 type "S" load cell limited to 10 kg, fixed to the test bench structure (see Figure 5.2). These cells utilize a spring that deforms elastically when subjected to a load. The engine's pulsating jet propels the load cell forward via a steel cable, causing deformation in the spring, which is detected by strain gauges on the spring element. This deformation is then converted into an electrical signal, and the HX711 amplifier is employed to convert this signal from the load cell into a digital format.

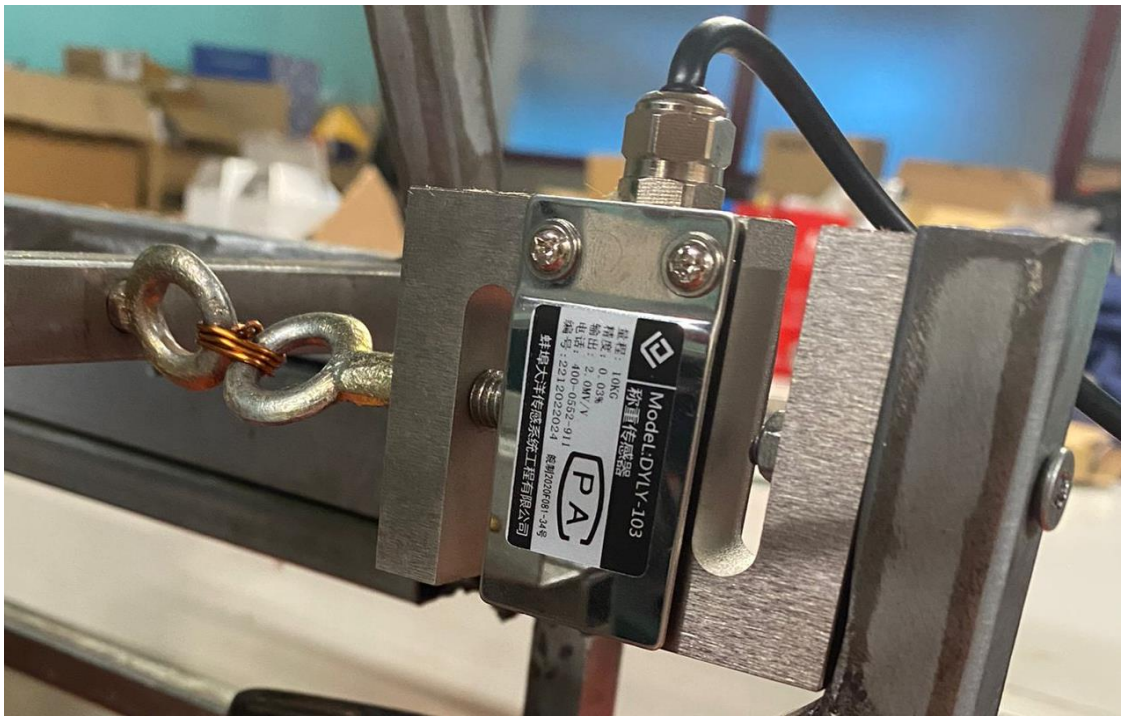

Figure 5.2- Load Cell DYLY-103.

5.1.3. Fuel Mass Flow

To quantify the fuel mass flow rates during tests involving gasoline, an indirect assessment method was employed by altering the mass of the fuel tank. This involved utilizing a specialized 16×16 mm square-profile platform engineered at the UBI laboratory (see Figure 5.3). The platform was integrated with a DYLY-103 type “S” load cell capable of accommodating loads up to 20 kg. Real-time fluctuations in mass were captured by this load cell through the HX711 amplifier.

1. Load Cell
2. Platform

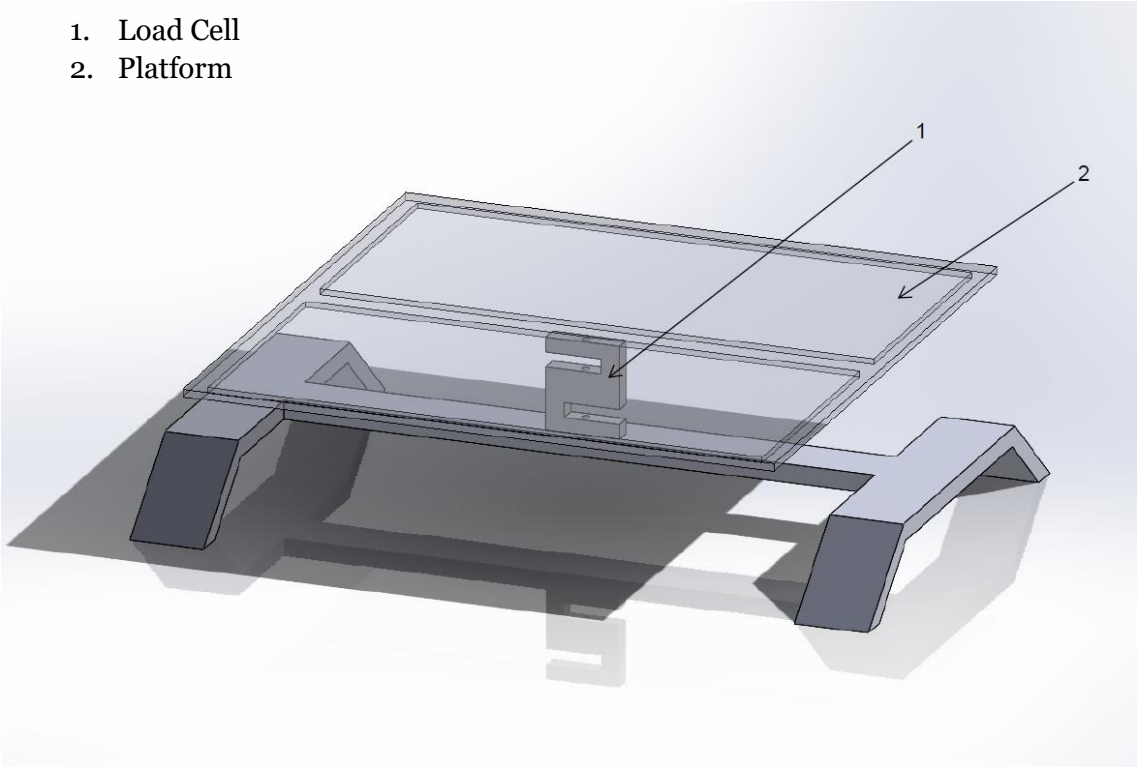

Figure 5.3- Platform for measuring fuel flow in real time.

5.1.4. Frequency of Operation

When contemplating the design of a pulsejet, it is essential to bear in mind that these devices operate under the influence of an intricate between fluid thermodynamics and acoustics. In acoustic terms, assessing the performance of a deflagration engine and understanding its geometry requires knowledge of its operational frequency.

To accomplish this objective, the audio produced by the pulsejet was captured during the experiments utilizing a smartphone positioned at a safe distance, ensuring the preservation of the device's integrity.

Subsequently, the gathered data underwent analysis utilizing MATLAB code supplied by Salvado [32]. This analysis facilitated the deduction of the actual operational frequency, enabling a comparative assessment against the values computed employing the methodology detailed in section 3.9. The operational frequency is determined by utilizing the MATLAB DFT (Discrete Fourier Transform) operator, which converts the time signal captured by the smartphone's microphone into a signal within the frequency domain.

5.2. Experimental Procedure for data Acquisition

The UBI propulsion laboratory conducted static tests aimed at evaluating the pulsejet engine's performance. However, owing to safety concerns associated with the emission of exhaust gases, the tests had to be conducted in an outdoor setting. Table 5.1 provided encapsulates the pertinent characteristics of the air environment observed during these tests.

Table 5.1-Ambient air properties during static tests.

Air Properties		
Covilhã Altitude	700	m
Atmospheric Pressure	93194	Pa
16/11/2023		
Temperature	286.15	K
Humidity	50	%
23/11/2023		
Temperature	285.45	K
Humidity	45	%
28/11/2023		
Temperature	284.75	K
Humidity	81	%

Before commencing the experiments, precautions were implemented to ensure the absence of high-voltage currents within the system and its various components upon activating the ignition module. Hence, measures were taken to isolate potential current paths between the metallic structure and the sensors to prevent any impact on data measurements.

The outdoor experiments took into account the wind direction for safeguarding materials and maintaining operator safety. Furthermore, a complete set of safety protocols was in place, encompassing the fastening of the pulsejet to the test bench, the utilization of heat-resistant gloves to withstand elevated temperatures, and the implementation of noise-cancelling hearing protection to mitigate the engines' inherent high noise levels.

After verifying all the specified conditions, the tests proceeded in the subsequent chronological sequence:

- Electric discharge at the spark plug
- Injection of C_3H_8
- Force compressed air into the intake

- Gasoline injection starts when the pulsejet achieves self-sustaining capability using C_3H_8
- Gradually reduce the flow rate of C_3H_8 to zero.

During testing, the combustion chamber walls approached the melting temperature of steel, becoming incandescent, as shown in Figure 5.4. Despite the sequential testing procedure described above requiring time, the static tests during the pulsejet's self-sustainability phase were limited to approximately 4 minutes to prevent compromising the steel's integrity.

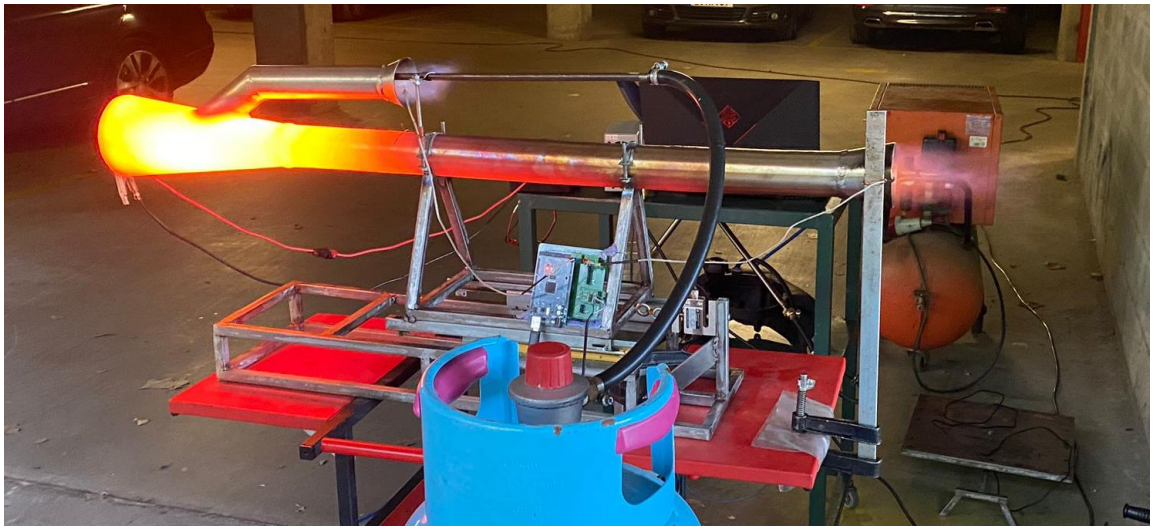

Figure 5.4-Pulsejet during a static test.

To comprehend the propellant's characteristics, diverse test scenarios were conducted, altering the fuel type between propane and gasoline while varying the mass flow rates. To capture the engine's performance metrics, temperatures sensors were installed in the intake (Temperature-1) and in the exhaust (Temperature-2). Load cells facilitated the measurement of traction force and fuel mass flow rate. These tests also allowed for the determination of the engine's operational frequency.

Through programming code created within the ARDUINO IDE-version 2.1.1 (Appendix A), the sensors connected to an Arduino Mega 2560 board were utilized for data collection and storage, excluding the smartphone (Appendix C). However, the smartphone was employed specifically for audio recording to determine the frequency using MATLAB code. In Figure 5.5 the experimental apparatus for data acquisition is depicted.

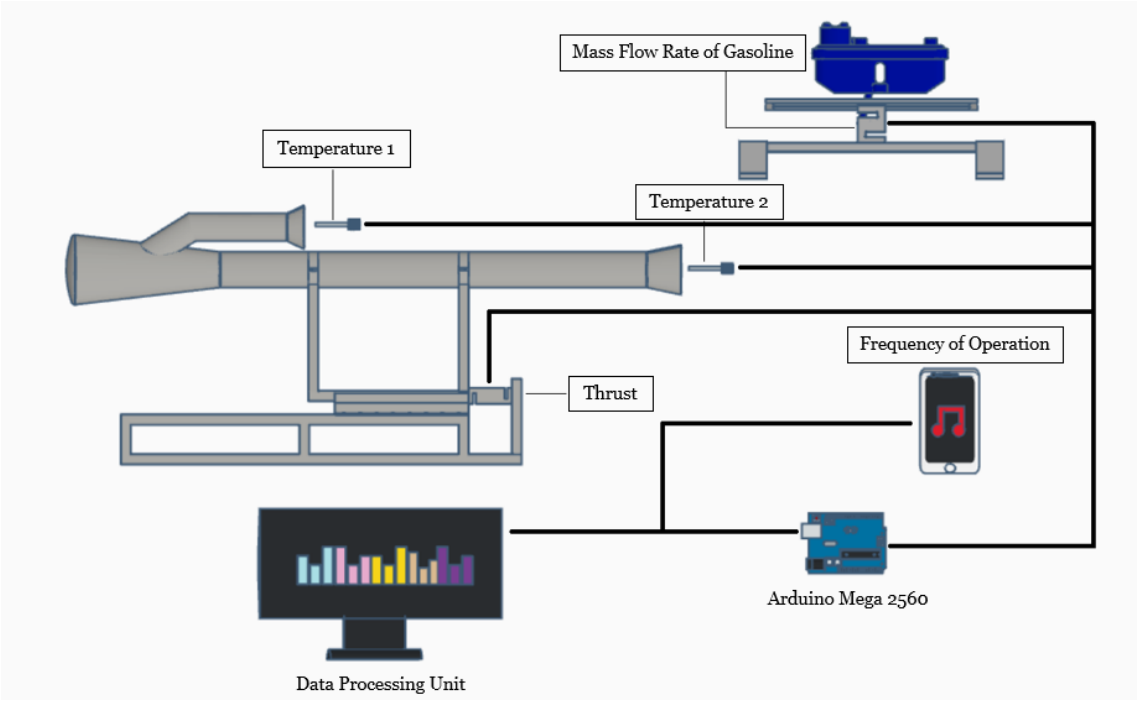

Figure 5.5- Experimental apparatus for data acquisition.

5.3. Outcomes

The following findings from static pulsejet experiments involving gasoline and propane are detailed below. Gasoline tests utilized a single nozzle but allowed for the adjustment of flow rates via the ball valve. Conversely, only one valid test was conducted for propane.

This analysis facilitates an examination of the engine's performance and its behaviour when operated with two distinct fuel types. Notably, in all trials, the self-sustaining effect was achieved. Nevertheless, the initial characteristic pulses inherent to this engine type were evident until stable operation was achieved.

5.3.1. Fuel Mass Flow

5.3.1.1. Propane

The pulsejet's fuel mass flow rate, powered by propane during testing, was determined by measuring the initial and final weights on a scale. This measurement, along with the duration of the test allowed for an estimation of the fuel flow rate. Consequently, the propane mass flow rate utilized in this test was calculated to be 2.54 g/s.

5.3.1.2. Gasoline

To document mass variations in real-time during the gasoline tests, an alternative approach was employed, detailed in section 5.1.3. The resulting data were entered into Microsoft Excel spreadsheets for further analysis.

Each data point depicted in Figure 5.6 corresponds to the mass measurement of the tank, pump, and fuel assembly. Employing the capabilities of Excel enabled the derivation of a linear trend line. The robustness of this methodology is evident from the R-squared value, which closely approaches 1, underscoring its reliability.

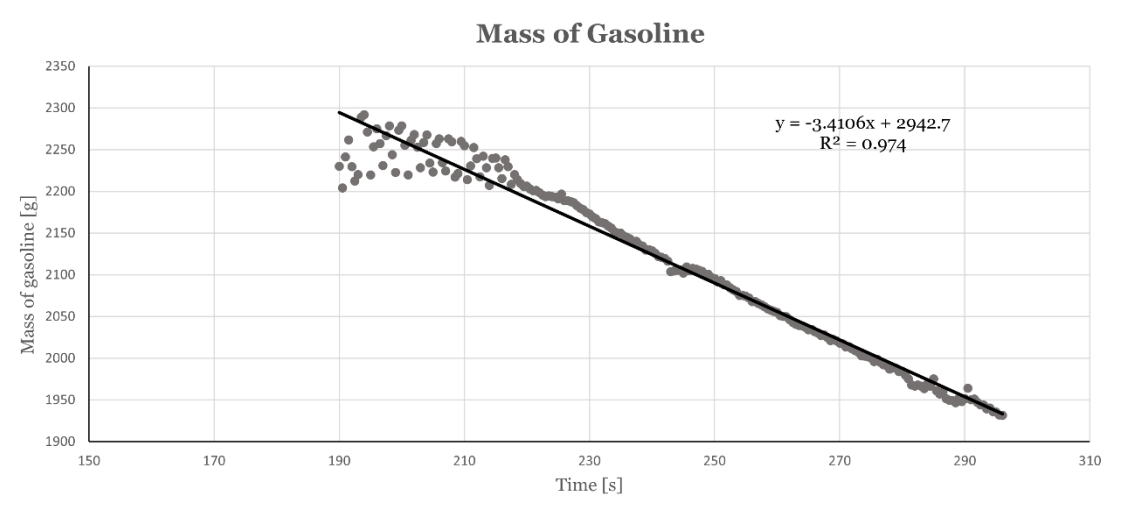

Figure 5.6- Temporal fluctuations in the mass of the Tank, Pump, and Gasoline assembly.

Hence, the average rate of fuel change is determined by the gradient of the trend line, which possesses an absolute value of 3.41 g/s. The consistent approach was applied throughout the remaining tests utilizing gasoline as the fuel source.

5.3.2. Temperature

Thermocouples positioned equidistantly upstream and downstream facilitated the observation of the progressive changes in temperature within both the intake and exhaust ducts.

5.3.2.1. Propane

In Figure 5.7, the progression of exhaust and intake temperatures across time is depicted. The initial 170 s exhibit intermittent pulsations, typical of the early phase of the pulsejet functioning. While the exhaust temperature steadily rises, the intake temperature remains consistent due to the compressed air cooling the surrounding ambient air. After this period, the engine walls attained a sufficiently elevated temperature, enabling a steady-state operation at a constant thrust.

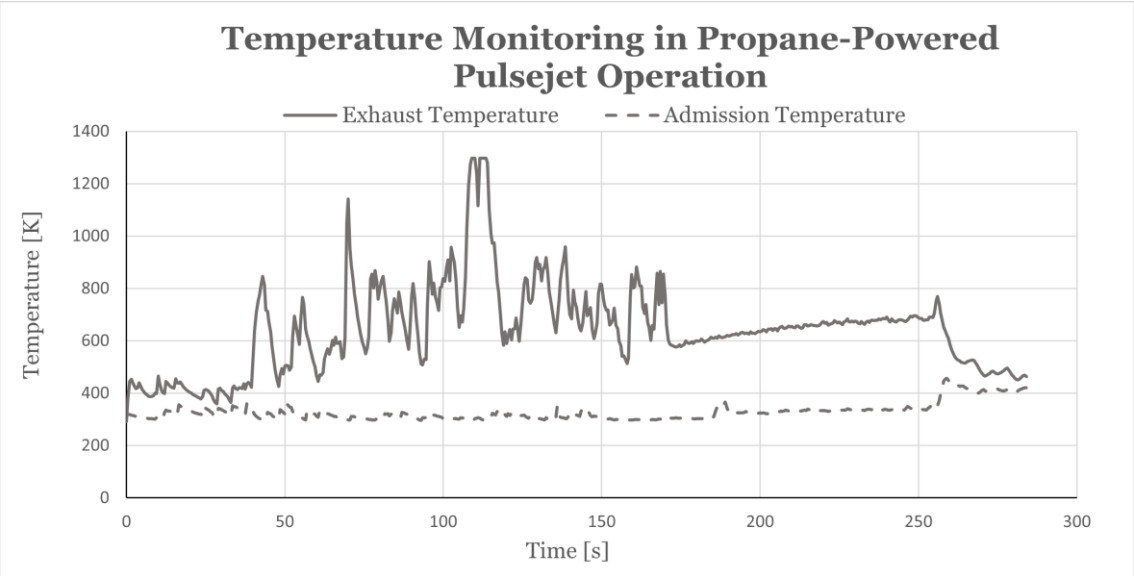

Figure 5.7-Temperature changes in Intake and Exhaust over time with the pulsejet running on Propane.

During the time interval spanning from 170 to 250 seconds, the recorded duration signifies the consistent and stable performance of the propellant in the conducted experiment. Within this phase, the compressed air is removed, and the ignition module is switched off.

After 250 seconds, there is a sudden temperature increase followed by a decline, a common pattern when a pulsejet fails to sustain a stable thermodynamic cycle. When a pulsejet stops, the fuel supply is interrupted, but there might still be unburned fuel in the exhaust duct or in the combustion chamber, causing a temporary combustion.

5.3.2.2. Gasoline

As previously noted, when gasoline is used as fuel in tests, the engine walls are initially heated to aid the start-up of the liquid fuel pulsejet. The Figure 5.8 illustrates the stage during which the engine solely operated on gasoline.

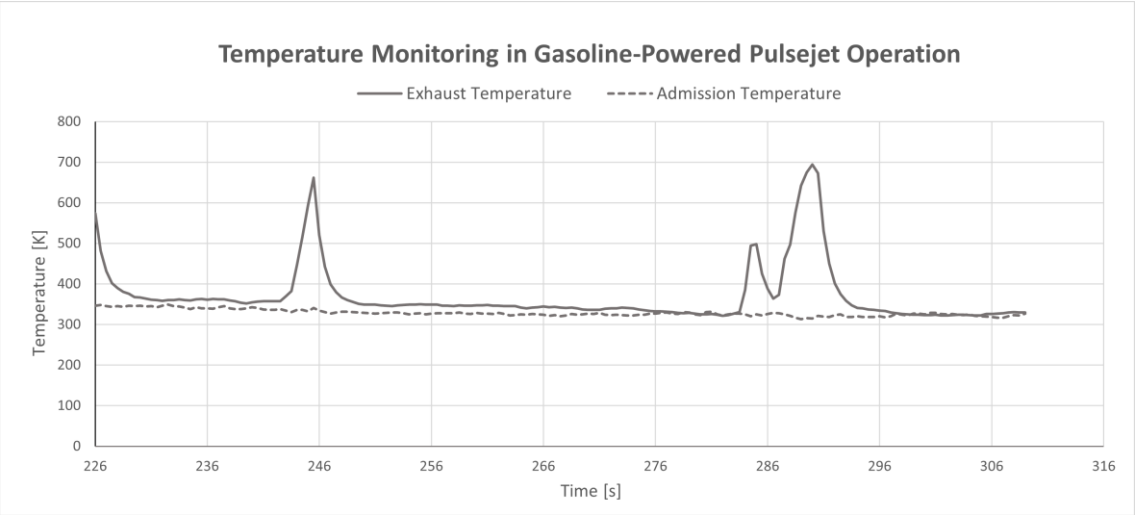

Figure 5.8- Temperature changes in Intake and Exhaust over time with the pulsejet running on Gasoline.

It is verified that initially, the temperatures are higher than in the test using propane. These temperatures remain practically constant throughout the engine's operation.

Note that in the test of the engine running on propane, during the self-sustainability phase, the average exhaust and intake temperatures are 617 K and 350 K, respectively. However, in the test of the pulsejet running on gasoline, the average exhaust and intake temperatures are 369 K and 324 K, respectively. There is a decrease in the combustion gas temperature, despite preheating the pulsejet to run on gasoline. This reduction is attributed to the gasoline/air mixture being lean, leading to a decrease in combustion temperatures.

Furthermore, it is observed that the exhaust and intake temperatures are very close, indicating unstable combustion. The peaks in exhaust temperature are attributed to the engine's inability to operate under a stable cycle, resulting in uncontrolled residual combustion. This could suggest that the mixture was inadequate.

5.3.3. Thrust

The load cell installed on the workbench described in section 4.3 allowed for the recording of the thrust values for both propane and gasoline tests.

5.3.3.1. Propane

In Figure 5.9 the values of thrust produced by the pulsejet running on propane are presented over time. Similar to the temperature recording in this experiment, the initial

170 s also refer to the initiation, characterized by a pulsating regime. Between 170 s and 250 s corresponds to the self-sustaining operation of the engine.

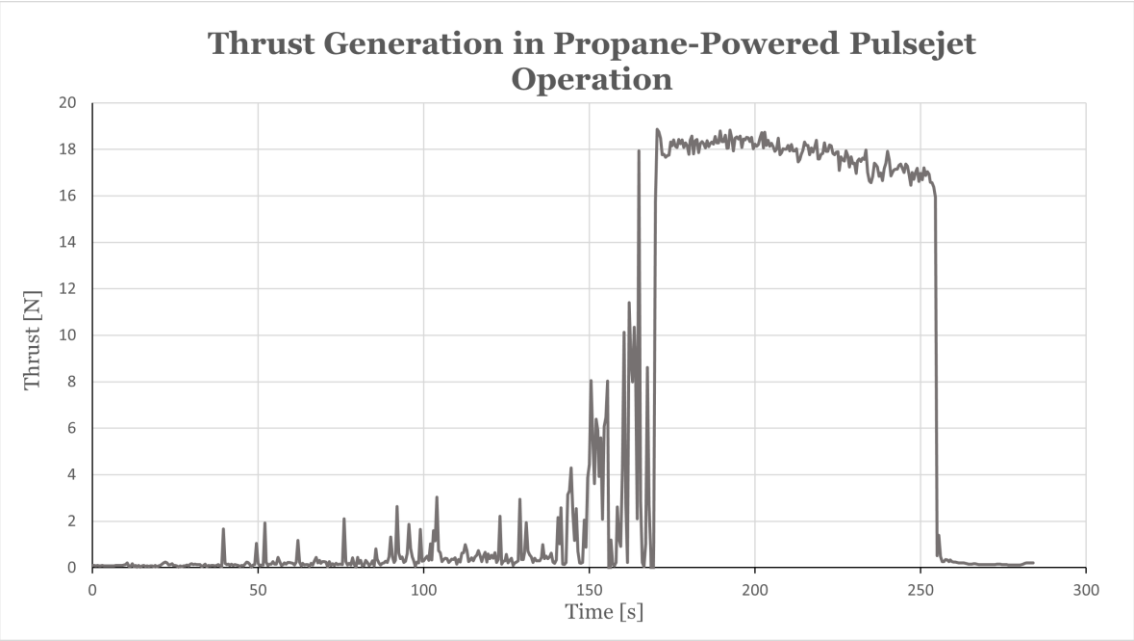

Figure 5.9-Thrust generated by the Propane-Powered Pulsejet over time.

An experiment was conducted involving the engine operating on propane, exceeded the mentioned values, producing a maximum thrust of 37.35 N (see Figure 5.10). However, this specific trial was disregarded in the analysis due to the displacement to the thermocouple responsible for measuring exhaust temperatures. The displacement resulted from the high flow velocity, causing the thermocouple to register only ambient temperature readings.

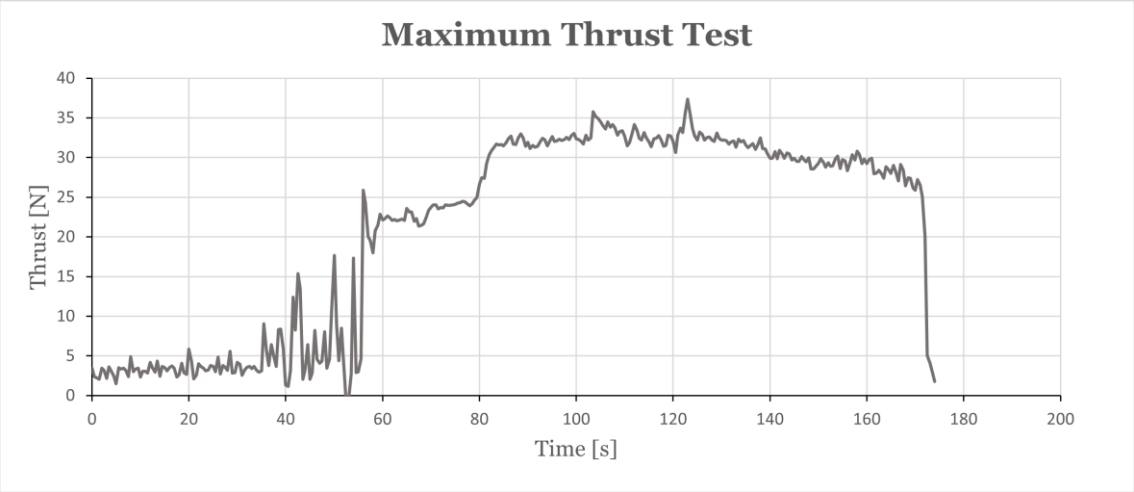

Figure 5.10-Maximum thrust test generated by the Propane-Powered Pulsejet over time.

This test allowed to surpass Duarte's [6] experimental value, achieving 26.14 N of maximum static thrust. This indicates that the geometry of the studied pulsejet was optimized. However, it was not possible to exceed the maximum static thrust predicted but the theory mentioned in section 3.10, which is 53.46 N.

Please note that this test was successful potentially because a filled propane cylinder was utilized, resulting in higher pressure during fuel injection.

5.3.3.2. Gasoline

Regarding the gasoline trial conducted, the thrust values were documented in Figure 5.11 similar to the temperature graph for this test, the analysis is confined to the phase during which the engine operates on gasoline. Three instances of thrust loss were observed, requiring the introduction of compressed air. Despite this instability, it was possible to achieve a self-sustaining effect between 244 s and 281 s.

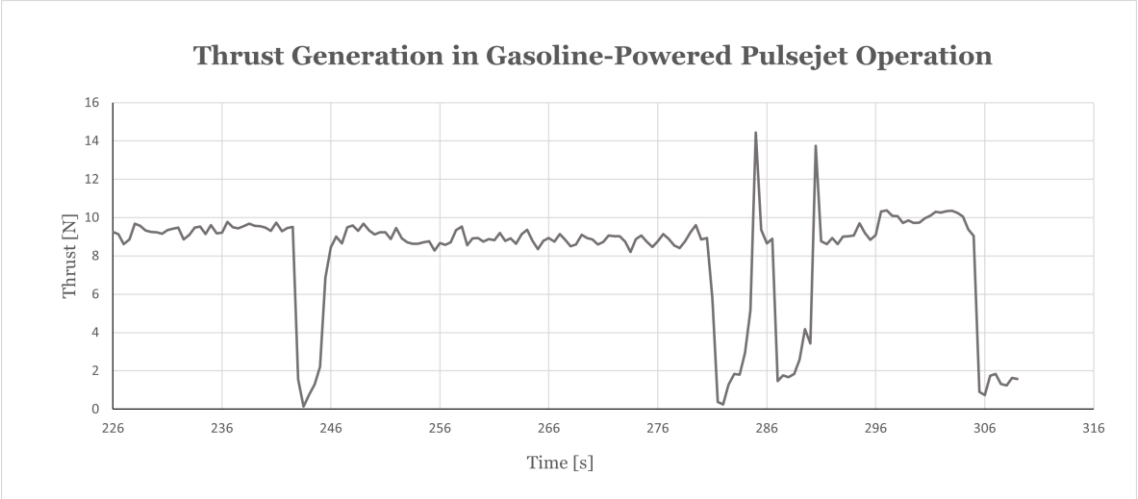

Figure 5.11-Thrust generated by the Gasoline-Powered Pulsejet over time.

In Figure 5.12, thrust values of the same test are recorded throughout the entire operational cycle. During the initial 150 s, the engine solely operated on propane, initially functioning through intermittent pulsations, stabilizing at a consistent thrust of 19 N from the 104 s. Subsequently, as the pulsejet's operational temperature increased and the combustion chamber walls became incandescent, the liquid fuel injection system was activated. The introduction of the fuel resulted in some combustion instability, requiring the application of compressed air. This phase lasted from 150 s to 226 s, during which the propane flow was gradually decreased. Beyond the 226th second, the engine exclusively ran on gasoline.

With Figure 5.12, it is possible to observe more clearly the behaviour of the pulsejet with different types of fuel. It is evident that the engine, when operating with gaseous fuel, exhibits better performance than when using liquid fuel. The pulsejet's maximum static thrust while operating on gasoline decreases by approximately 29% compared to the period of operation on propane.

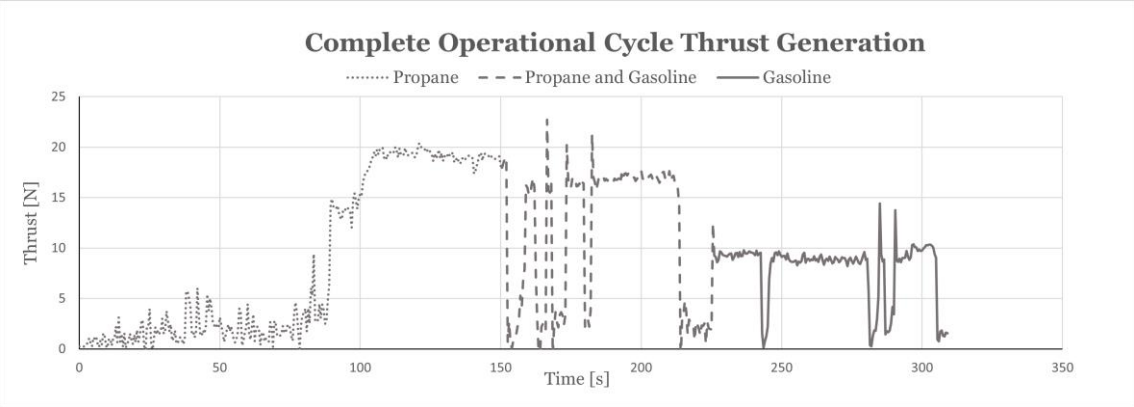

Figure 5.12- Thrust generated by the pulsejet during all operational stages, aiming to preheat the engine with propane for self-sustainability using only Gasoline.

As demonstrated by Li et al. [30] in their experimental study, pulse combustion is sustained by thermoacoustic oscillations influenced by the intake process. Inadequate mixing of the fuel mixture leads to combustions instabilities. Hence, the considerable loss of thrust is justified by the insufficient atomization.

Despite using a 10-bar pump, the fuel was only atomized at 8 bar, as mentioned in section 4.6.2. The inadequate atomization process led to the formation of larger fuel droplets and an uneven distribution of particles. Consequently, this uneven distribution led to areas of concentrated fuel surrounded by excess air in the combustion chamber, resulting in incomplete combustion due to insufficient fuel in relation to available oxygen. As result, energy production decreased, combustion efficiency reduced, potentially causing increased emissions due to incomplete fuel combustion.

However, despite the valveless pulsejet behaving erratically when running on gasoline, showing unpredictable filling sequences, swift combustion, and fluctuating speeds in expelling the resulting products, the self-sustaining effect was achieved. This reinforces Anand's et al. [14] experimental study, where sustained instability was achievable for valved pulsejets.

5.3.4. Fuel Consumption

To comprehend the efficiency of the valveless pulsejet and quantify the fuel usage, the specific thrust fuel consumption for each test was calculated using the formula 3.12 mentioned in section 3.8.2.

5.3.4.1. Propane

The studied pulsejet produced an average thrust of 15.91 N with a propane flow rate of 2.54 g/s, while achieving a maximum static thrust of 18.86 N in the same test. The fuel consumption rate to achieve this thrust was measured at 0.574 kg/N.h.

When compared to Duarte's [6] calculated trend line for thrust concerning the propane flow rate of 2.54 g/s in his experimental work, a reduced thrust was observed. This affirms an enhancement in the geometry, supported by the lower TSFC value, signifying the superior efficiency of the investigated pulsejet in contrast to Duarte's design.

5.3.4.2. Gasoline

In Figure 5.13, the observation of the three experiments conducted on the valveless pulsejet utilizing gasoline reveals that an elevation in the mass flow rate corresponds to an increase in the generated maximum static thrust.

However, concerning the average thrust, the test in which 2.34 g/s of fuel was dispensed generated 8.42 N, while the test that dispensed 3.41 g/s produced 8.00 N. Despite a significant increase in flow rate, there was a decrease in the generated thrust. This was likely due to the differing initial conditions of each test. Both experiments were conducted on the same day, ensuring identical environmental conditions. However, in the trial that resulted in higher thrust, the initial and operating temperatures were higher, aiding in fuel vaporization and subsequently in the air/fuel mixture.

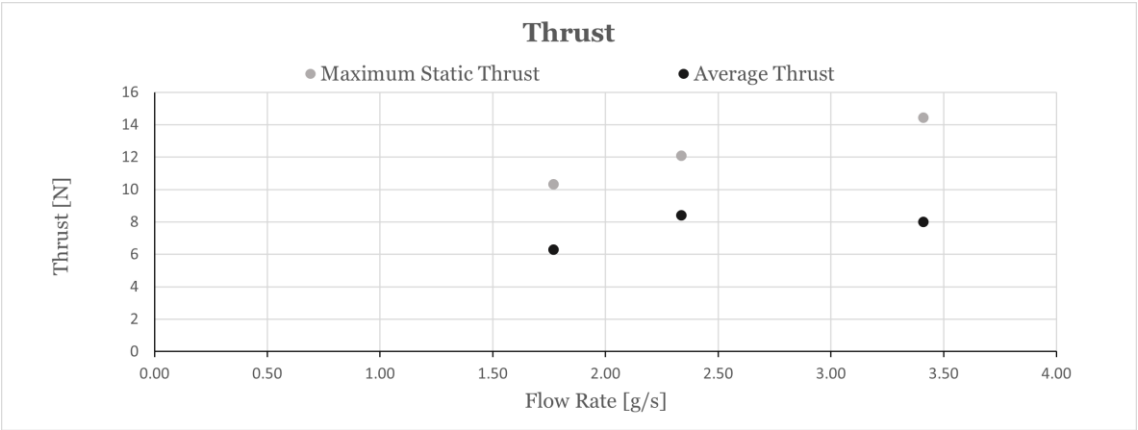

Figure 5.13-Comparison of Average and Maximum Static Thrust values across varied Flow Rates in three Valveless Pulsejet tests.

Table 5.2 exhibits the TSFC values observed during the gasoline-powered tests. Upon comparison with the propane-fuels test and Duarte's investigation, a discernible elevation in TSFC is evident. This indicates reduced efficiency of the pulsejet when operating on gasoline, signifying an increased fuel consumption to attain a particular thrust output. However, closer examination of the table for lower flow rates reveals a more effective combustion of the propellant responsible for generating thrust.

Table 5.2- Specific Thrust Fuel Consumption (TSFC) of the pulsejet.

Flow Rate [g/s]	Maximum Static Thrust [N]	Avarege Thrust [N]	TSFC [kg/N.h]
1.77	10.32	6.30	1.01
2.34	12.08	8.42	1.00
3.41	14.43	8.00	1.54

Therefore, it can be stated that the increase in generated thrust does not depend solely on the increase in the injected flow rate, there are other factors that need to be considered.

5.3.5. Frequency

The operational frequency of the valveless pulsejet was calculated using a MATLAB DFT operator to convert the signal from the time domain captured by the smartphone's microphone into a frequency domain signal.

Through Audacity 3.3.3, it was possible to edit some parameters of the recorded audio form each test, facilitating their analysis in MATLAB. Furthermore, employing the program provided by Salvado [32] allowed for the determination of the number of cycles performed by the engine per unit of time.

5.3.5.1. Propane

In depicted Figure 5.14, an observation was made regarding the operational frequency of the propane-fuelled pulsejet, which bears a resemblance to a Fourier series. This series constitutes a periodic function and is constructed through the combination of sine and cosine functions, commonly referred to as harmonics. In this particular scenario, the observed pattern approximates a square wave, theoretically achieved by a composite of sine functions of different frequencies.

From the Figure 5.14, it is also noticeable that within the period of 0,0226 s , three cycles were recorded, indicating that each cycle spans 0.008 s. Furthermore, within each cycle,

multiple peaks with varying amplitudes are observed, possibly linked to harmonic frequencies. It can also be observed that there are two sound waves associated with the waves released during intake and exhaust.

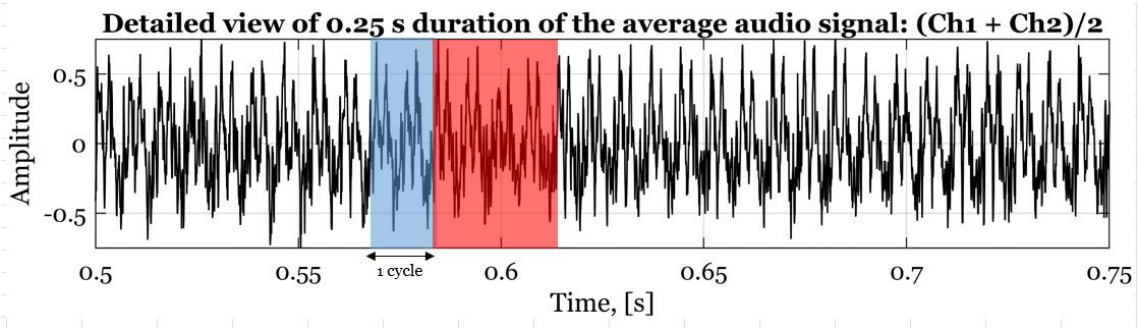

Figure 5.14-Audio Amplitude-Time graph during the propane-powered engine operation.

A typical amplitude spectrum using Discrete Fourier Transform (DFT) of an audio is shown in Figure 5.15. The DFT demonstrates that the dominant frequency for the conditions of the test was 132.77 Hz. As earlier mentioned, this signal exhibits frequencies that are multiples of the fundamental frequency, termed as harmonics. Notably, there are six harmonics present, considering the remaining noise signal. The DFT graph reveals that the second frequency is at 265.55 Hz. The third harmonic was found to be almost three times the fundamental frequency of the jet, at 398.42 Hz. The fourth and fifth harmonics are at 532.14 Hz and 664.67 Hz, respectively. The last harmonic has a frequency of 794.11 Hz.

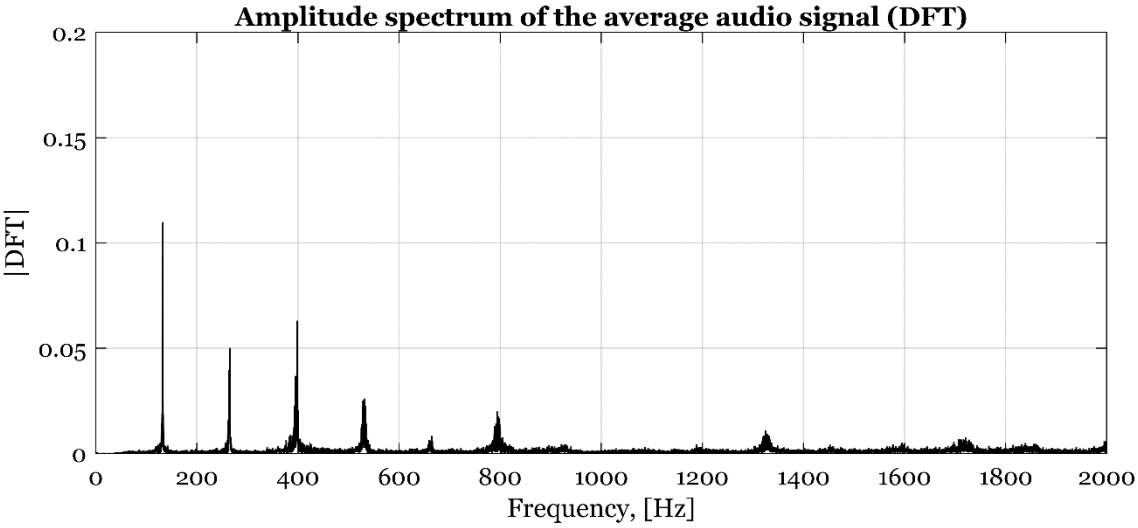

Figure 5.15- Amplitude Spectrum of as function of Frequency of the engine running on propane.

The acoustic theory will be briefly discussed here. The half-wave theory aims to describe the pulsejet as a half-wave resonator, in other words, as a tube open at both ends. As mentioned in section 3.9, the distance between the combustion chamber (pressure

antinode) and the end of the exhaust pipe (pressure node) determines the fundamental wavelength that governs the engine. Meanwhile, the distance between the chamber and the end of the intake accommodates a secondary wavelength, which should be an odd harmonic of the fundamental.

Although an open tube is not traditionally a quarter-wave resonator, it is more accurate to consider a valveless engine as two quarter-wave oscillators mounted against each other. For this geometry, the engine has a pressure antinode in the center and a node at each end, explaining the presence of various harmonics.

According to Ogorelec [4], for proper operation, the length of the exhaust pipe should be an odd multiple of the length of the intake pipe. However, this length varies with temperature and is not uniform throughout the engine.

5.3.5.2. Gasoline

For the tests with the engine running on gasoline, the procedure was the same. Figure 5.16 shows the operational cycle of the pulsejet through the audio signal. The behaviours of the engine running on liquid and gaseous fuel are quite similar. One operational cycle displays a square wave pattern, with a period of 0.00817s.

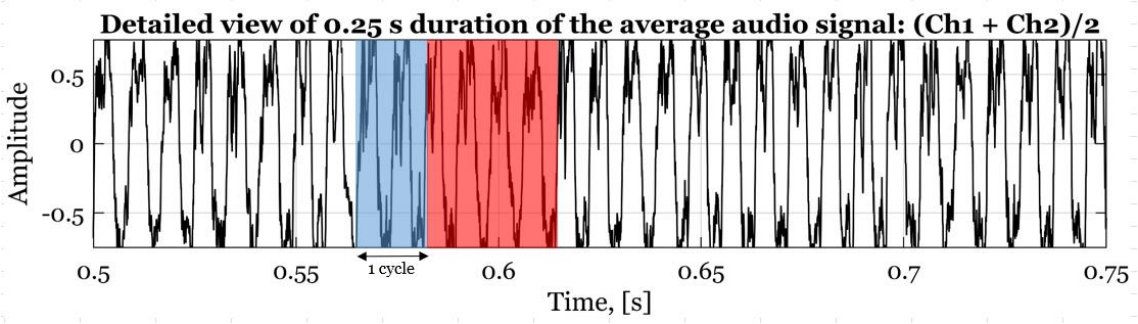

Figure 5.16-Audio Amplitude-Time graph during the gasoline-powered engine operation.

Regarding the amplitude spectrum shown in Figure 5.17, some differences are noticeable. During this specific test the 4^{th} and 5^{th} order harmonics are not as prominently observable as they were in the test conducted with propane. This variation may be attributed to the position of the data acquisition device since the other tests conducted with gasoline showed six visible harmonics.

The DFT revealed that the predominant frequency of the engine was at 122.38 Hz in the amplitude spectrum. The second harmonic is approximately twice the operational frequency, namely 244.76 Hz. The third harmonic is at 367.14 Hz in the amplitude spectrum. The fourth and fifth harmonics are theoretically at 489.52 Hz and 734.28 Hz, respectively. The last harmonic has a frequency of 734.28 Hz.

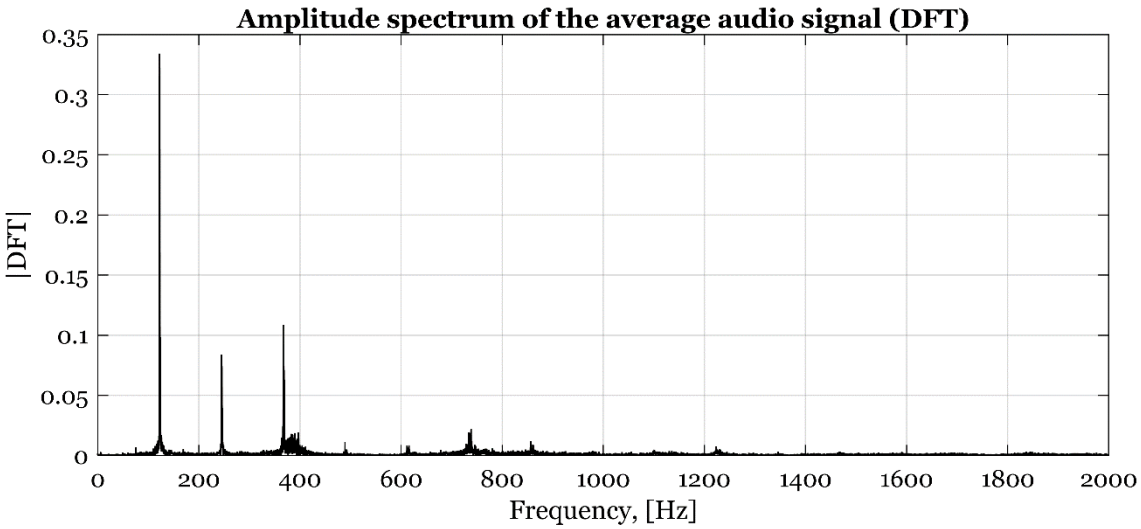

Figure 5.17-Amplitude Spectrum of as function of Frequency of the engine running on gasoline.

To understand how the change in fuel flow affects the operational frequency of the valveless pulsejet, the frequency data is presented in Figure 5.18, including both the experimental results and those obtained through the method described in section 3.9. The latter suggests an average between the cycles executed by the intake and exhaust.

It is worth noting that in the test where the flow rate was 1.77 g/s, it was not possible to calculate the theoretical frequency because the exhaust thermocouple did not measure the temperature of the exhaust gases. Nevertheless, this test was still considered.

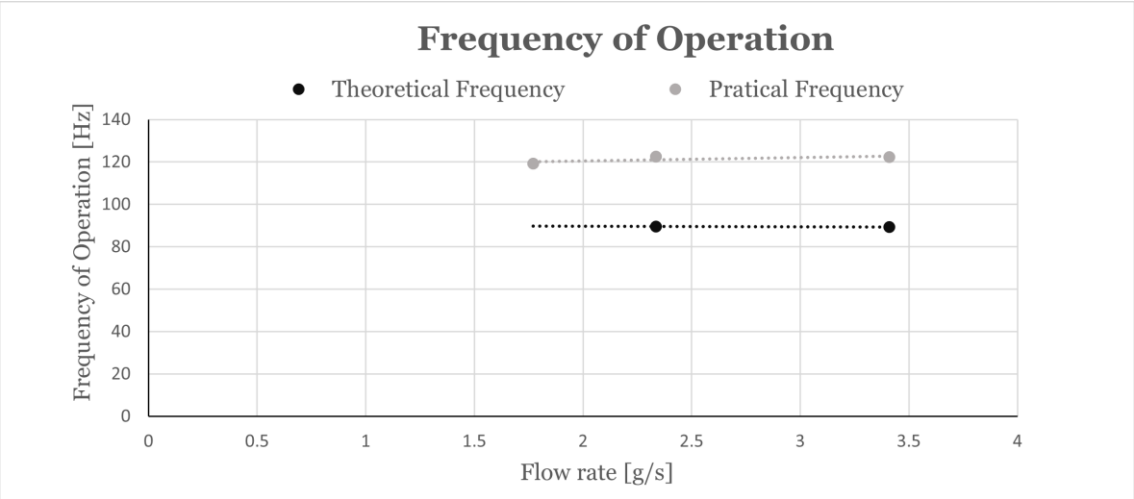

Figure 5.18- Experimental Frequency vs Theorical Frequency in the trial of the engine running on gasoline.

The graph in Figure 5.18 shows a notable disparity between the frequency calculated through theory and the frequency observed in experimental tests. The calculated frequency displayed a maximum error of 26% compared to the measured frequency, aligning with findings reported by Duarte [6].

The experimental frequency remained constant around 121 Hz for different defined mass flow rates, indicating that the valveless pulsejet's operating frequency is primarily influenced by its geometry, aligning with McCalley's [12] practical study.

However, in the propane trial, the operational frequency exhibited a slight increase compared to the gasoline trials. This phenomenon can be elucidated by analyzing the subsequent graph:

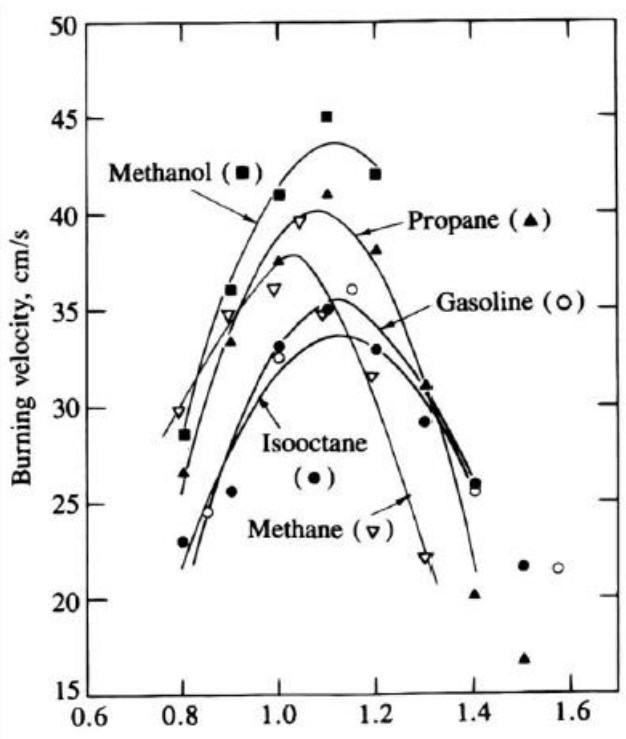

Figure 5.19- Burning velocity for different species and fuel/air ratio [31].

As demonstrated in Figure 5.19, the burning speed of propane is faster compared to that of gasoline. When the equivalence ratio approaches the stoichiometric value, the flame speed increases while the flame length and delay decrease [31]. Conversely, a reduction in flame speed extends the duration of each cycle, leading to a decrease in the operational frequency.

Chapter 6

6.Conclusions and Future Work

With the development of this project, it was possible to study and understand the operation of a valveless Chinese-type pulsejet. The final chapter aims to present the conclusions resulting from the static tests. Finally, possible projects that could be developed in the future will be presented.

6.1. Conclusions

This project ensued from Duarte's [6] experimental study, which focused on constructing a Chinese-type pulsejet functioning on propane. The advancements made in prior research allowed for the optimization of geometry, facilitating the development of a Chinese-type pulsejet capable of operating with liquid fuel, specifically gasoline.

Overall, despite encountering some adversities, it was possible to achieve a significant portion of the proposed objectives. Initially, the intention was solely to test a type of fuel and compare the behaviours of the pulsejet with the experimental studies conducted at UBI, given the very similar geometry. However, to comprehend the improvements made to the geometry, a test with propane was made. It was discovered that the engine under study exhibited better performance. This was primarily due to the grinding of the interior welds, preventing discontinuities within the welding region. It was noted that the material used had a significant impact on the engine's performance, allowing for longer testing periods due to the capability of stainless steel 1.4835 to withstand high temperatures without compromising the engine's structural integrity.

Regarding the data acquisition system, there were some experimental limitations that hindered comprehensive data collection. Specifically, the high temperatures reached by the engine demanded sensors capable of withstanding such severe conditions. It was not possible to monitor the internal pressure in the combustion chamber or the temperature. Additionally, the sound pressure level of the pulsejet was not recorded. However, with the available data, a rigorous analysis was conducted, enabling the observation of typical behaviours of a valveless pulsejet.

One of the main challenges faced during this project was the initiation of the gasoline-powered engine. It was found that the engine needs to be preheated, indicating that the walls of the pulsejet needed to be warm to facilitate fuel vaporization and subsequent mixing. Therefore, it was necessary to start the engine using propane to raise the temperatures of both the liquid fuel and the pulsejet structure, similar to the procedure undertaken by McCalley [12] in his practical work.

Concerning the injection system designed for this engine, its performance fell significantly below anticipated levels owing to insufficient pressure. The low pressure supplied by the pump influenced all the operational data since the fuel atomization was inadequate. The pressure gauge installed indicated that the system was operating at only 8 bar. This caused in larger-than-optimal fuel droplets, hindering vaporization process, and consequently affecting the mixture formation. This issue occurred because a fixed-displacement pump was used, the only available option at that time. It is believed that changing the pump would have beneficial effects on the efficiency of the pulsejet.

Despite this obstacle, the self-sustaining effect was achieved for both fuels. It was also found that the optimal position for injection was identified as being in the middle of the intake tube, for both gaseous and liquid fuel. This approach allowed for a better mixture with the incoming air and the injected fuel.

In terms of environmental conditions, the valid tests were conducted on three different days. It was observed that a more humid environment tended to negatively affect the jet efficiency. Humid air contains a higher amount of water, reducing the engine's efficiency due to reduced air mass available for combustion compared to dry air. Concerning temperature, theoretically, at lower ambient temperatures, the engine's efficiency tends to increase because the air is denser, resulting in a greater mass of being admitted. This effect was not evident. However, the low temperatures caused a decrease in the internal pressure of the propane tank. Consequently, there was reduction in propane flow rate, resulting in greater difficulty in starting the engine.

With the data analysis presented in Chapter 5, it was proven that the engine running on propane performs better than when using gasoline. In fact, even with preheating of the pulsejet during the gasoline tests, the operating temperature was lower compared to the

test conducted using propane. Additionally, it was observed that the exhaust and intake temperatures during the gasoline test were very close, indicating unstable combustion.

In the gasoline test compared to the one using propane, there was a decrease of approximately 52% in the average thrust produced. Concerning the maximum static thrust in the gasoline tests, an increase in the flow rate resulted in an augmentation of force; however, this escalation didn't have a similar effect on the average thrust. This suggests that the average thrust doesn't rely solely on the injected flow rate but also on the quality of the mixture. Nevertheless, with an optimal mixture and a higher fuel flow rate, it could potentially generate more thrust and approach the predicted 53,46 N according to Tharratt's [22] method.

The TSFC values increased when switching from gaseous to liquid fuel, indicating that the engine was less efficient with gasoline. However, compared to the study conducted by Duarte [6], the test with propane showed improvements due to the optimization of the geometry.

Regarding the operational frequency, the amplitude-time graph displayed a resemblance to a periodic square wave comprising sine functions of varying frequencies for both gasoline and propane fuels. The DFT graph exhibited harmonics typical of a valveless pulsejet, with both gasoline and propane tests revealing six harmonics. In gasoline tests, an increase in the injected flow rate showed a nearly constant operational frequency, in line with McCalley's [12] theory of pulsejet behaviour being constrained by its geometry. In relation to the theory predicting the engine's operational frequency, an underestimation of the cycles performed per second was evident, revealing a maximum error of 26%.

However, in the propane test, the first harmonic was slightly higher compared to that observed in the gasoline tests. This was attributed to the fact that the burning speed of propane is faster compared to that of gasoline, leading to an increased number of cycles performed per second.

Conclusively, the selection of fuel for a given engine will have multifaceted effects on its operation. Primarily, regarding thermodynamic aspects, the choice of fuel will modify the flame temperature, similarly impacting the combustion rate and operational frequency. It is essential to note that not all types of fuels are compatible with the pulsejet, highlighting the criticality of understanding the combustion process and temporal delays in comprehending the engine's functionality [31].

6.2. Future Work

In accordance with what has been stated, the thrust force generated by the valveless pulsejet running on gasoline did not meet the expectations. Therefore, the initial suggestion for future work focuses on enhancing the injection system to enhance the performance and efficiency of this engine.

The deficiencies in the gasoline injection system were focused on the lack of pressure. Therefore, the primary recommendation would be to replace the fuel pump to achieve higher injection pressures. However, with this replacement, it is essential to change connections and materials, particularly hoses, to withstand the high pressure. Another way to achieve the ideal pressure would be to build a pressurized tank.

In order to study flow behaviours within the combustion chamber, it would be essential to invest in temperature and pressure sensors. A thermal sensor, like a "K" type thermocouple capable of measuring temperatures within the range of $[-260, 1260]\ °C$, would serve as a valuable tool in examining the observed phenomenon highlighted by Duarte [6]. He noticed that the temperature within the combustion chamber and the thrust exhibited a similar pattern, albeit for a different type of fuel. A pressure sensor like the Kulite XTE-190-50A, designed to withstand high temperatures and utilized by McCalley [12], would allow for the analysis of pressure evolution over time. This sensor would aid in determining the operational frequency of the pulsejet and facilitate a comparison with estimated values.

The operational frequency results were quite satisfactory; however, in order to study the sound pressure levels for various gasoline flow rates and to achieve greater precision in data collection, acquiring a sound level meter would be essential for future projects.

As seen by Bour [31] in his research, not all fuels are suitable for a specific geometry, depending on various geometric factors, notably the shape of the combustion chamber. In order to better understand this fuel exchange, a new CFD study should be conducted to optimize the geometry for liquid fuels.

As a means to complement the research, it would be pertinent to conduct an experimental study to assess the impacts caused by variations in the tail and combustor lengths on the operability and efficiency of a valveless pulsejet engine.

Bibliography

[1] A. F. El-Sayed, “Pulsejet, Ramjet, and Scramjet Engines” in *Fundamentals of Aircraft and Rocket Propulsion*. London: Springer, 2016, pp. 315-226.

[2] G. D. Roy, S. M. Frolov, A. A. Borisov, and D. W. Netzer, “Pulse detonation propulsion: Challenges, current status, and future perspective,” *Prog Energy Combust Sci*, pp. 545–672, 2004.

[3] “The WWII V-1 Doodle Bug Flying Bomb.” [Online]. Available: www.fiddlersgreen.net/models/Aircraft/V1. Accessed on: April 1, 2023.

[4] B. Ogorelec, “Valveless Pulsejet Engines 1.5-a historical review of valveless pulsejet designs.”, 2005 [Online]. Available: http://www.pulse-jets.com/valveless/. Accessed: May 27, 2023.

[5] H. Sadig Hussain and A. Omer Ahmed, “Theoretical and Experimental Evaluation of Pulse Jet Engine,” University of Khartoum, 2008.

[6] Miguel Ângelo Lopes Duarte, “Construção e Ensaio Estático de um Pulsojato sem Válvulas,” Universidade da Beira Interior, Covilhã, 2020.

[7] A. Kudesia and A. M. Bisen, “FUTURE ASPECTS OF VALVELESS PULSE JET ENGINE”, *International Journal of Advanced Technology in Engineering and* Science, vol.3, 2015.

[8] Richard P. Ouellette, “Pulsejet ejector thrust augmentor,” US2005/0000221A1, 2005.

[9] C. Wenxiang, W. Xiaosong, W. Tao and S. Bo, “Numerical investigation of components length of china-type valveless pulsejet,” International Conference on Computational Intelligence and Software Engineering, 11-13 December 2009.

[10] Z. Tao, Z. Yong, and C. Wenxiang, “Numerical investigation of typical valveless pulse combustor working process,” *Energy Procedia*, vol. 141, pp. 287-291, 2017.

[11] T. Geng, F. Zheng, A. P. Kiker, A. V. Kuznetsov, and W. L. Roberts, “Experimental and numerical investigation of an 8-cm valveless pulsejet,” *Experimental Thermal and Fluid Science*, pp. 641–647, Jul. 2007.

[12] C. T. McCalley, “EXPERIMENTAL INVESTIGATIONS OF LIQUID FUELED PULSEJET ENGINES,” North Carolina State University, NC, 2006.

[13] J. K. R. Isac, L. Mohanraj, E. S. Sai, and V. K. Kannan, “Numerical simulation of a hydrocarbon fuelled valveless pulsejet,” *Propulsion and Power Research,* 2014.

[14] V. Anand *et al.*, “Visualization of Valved Pulsejet Combustors and Evidence of Compression Ignition,” *Flow Turbulence Combustion*, vol. 106, no. 3, pp. 901–924, Mar. 2021.

[15] D. R. Greatrix, *Powered Flight: The Engineering of Aerospace Propulsion*. Canada: Springer, 2012.

[16] M. Trancossi, O. Mohammedalamin, J. C. Páscoa, and F. Rodrigues, “Thermodynamic analysis and preliminary design of the cooling system of a pulsejet for aeronautic propulsion,” *International Journal of Heat and Technology*, 2016.

[17] R. S. Ismail, A. Jailani, and M. A. Haron, “Kadenancy effect, acoustical resonance effect valveless pulse jet engine,” in *AIP Conference Proceedings*, American Institute of Physics Inc., Sep. 2017.

[18] M. L. Coleman, “OVERVIEW OF PULSE DETONATION PROPULSION TECHNOLOGY,” Columbia: Chemical Propulsion Information Agency, 2001.

[19] C. Rajashekar, S. T. Aruna, M. J. R. Reddy, H. S. Raghukumar, and J. J. Isaac, “Studies on the Resonant, Combustion Flow Phenomena in a Small-Scale Quarts Glass Valveless Pulsejet Engine by High-Speed Flame Imaging using Chemical Tracers”, SIR-NAL Supra Institutional, 2015.

[20] “Lenoir Cycle.”. [Online] Available: https://www.hellenicaworld.com/Science/Physics/en/Lenoircycle.html. Accessed: Jul. 21, 2023.

[21] F. Zheng, R. L. Ordon, T. D. Scharton, A. V. Kuznetsov, and W. L. Roberts, “A new acoustic model for valveless pulsejets and its application to optimization thrust,” *Journal of Engineering for Gas Turbines and Power,* vol. 130, no. 4, 2008.

[22] C. E. Tharratt, “The Propulsive Duct: A Theoretical Approach to Assessing the Thermodynamic Process Within the Combustion Chamber of the Propulsive Duct, an Examination of the Potential of the Duct with Special Reference to the Application of Feedback and Spark Discharge Techniques,” *Aircraft Engineering and Aerospace Technology*, vol. 37, no. 11. pp. 327–337, 1965.

[23] "How to start a Pulsejet." [Online] Available: https://aardvark.co.nz/pjet/starting.shtml. Accessed: Aug. 27, 2023.

[24] A. Sofia Moura Melo "Pulsejet Engine Performance Estimation," Universidade da Beira Interior, Covilhã, 2019.

[25] A. Amezcua Sánchez, F. M. Ribeiro, and P. Brójo, "Design, construction and testing of a Pulsejet engine, "Universidade da Beira Interior, Covilhã, 2022.

[26] "Material Properties Database." [Online] Available: https://www.makeitfrom.com/material-group/Iron-Alloy. Accessed: Sept. 09, 2023.

[27] Nora-Silver, "Nozzles and Combustion Chambers" Chapter 5-Nozzles and Combustion Chambers.

[28] C. Jiang *et al.*, "Influence of Self-Pulsation on Atomization Characteristics of Gas-Centered Swirl Coaxial Injector," *Front Energy Res*, vol. 9, Sep. 2021.

[29] S. D. Sovani, P. E. Sojka, and A. H. Lefebvre, "Effervescent atomization." [Online]. Available: www.elsevier.com/locate/pecs. Accessed: Sept. 26, 2023.

[30] F. Li, M. Du, and L. Yang, "Effect of fuel injection parameters on performance characteristics and emissions of a thermoacoustic system," *Aerosp Sci Technol*, vol. 110, Mar. 2021.

[31] T. Bour and F. Coutand, "Theoretical and experimental investigation of the pulsejet engine," KTH School of Industrial Engineering and Management Energy Technology, Stockholm, 2016.

[32] Salvado, José António da Costa, "Decomposição de sinais acústicos em componentes independentes num DSP VLIW," *1º Workshop de Investigação e Desenvolvimento em Engenharia Eletrotécnica e das Telecomunicações-WIDEET'04,* Castelo Branco, 2004.

Appendix A

A. Arduino Code

```
#include "max6675.h"
#include "HX711.h"
//Thermocouple intake K
int thermoS0_1 = 43;
int thermoCS_1 = 45;
int thermoSCK_1 = 47;
float thermo_k_1;
MAX6675 thermocouple_1(thermoSCK_1, thermoCS_1,
thermoS0_1);
//Thermocouple exhaust K
int thermoS0_2 = 49;
int thermoCS_2 = 51;
int thermoSCK_2 = 53;
float thermo_k_2;
MAX6675 thermocouple_2(thermoSCK_2, thermoCS_2,
thermoS0_2);
// Loadcells
HX711 scale_1;
HX711 scale_2;
float reading_1;
float reading_2;
float traction1;
const int LOADCELL_DOUT_PIN_1 = 3;
const int LOADCELL_SCK_PIN_1 = 2;
const int LOADCELL_DOUT_PIN_2 = 5;
const int LOADCELL_SCK_PIN_2 = 4;
float Calibration1 = 437;
float Calibration2 = 415;
void setup() {
// Loadcells
scale_1.begin(LOADCELL_DOUT_PIN_1, LOADCELL_SCK_PIN_1);
scale_2.begin(LOADCELL_DOUT_PIN_2, LOADCELL_SCK_PIN_2);
scale_1.tare();
scale_2.tare();
scale_1.set_scale(Calibration1);
scale_2.set_scale(Calibration2);
Serial.begin (9600);
}
void loop() {
TRACTION();
FF();
TEMP();
SERIALCOM();
}
```

```
void TRACTION() {
reading_1 = scale_1.get_units();
traction1 = reading_1*9.81*0.001*-1;
}
void FF() {
reading_2 = scale_2.get_units();
}
void TEMP() {
thermo_k_1 = thermocouple_1.readCelsius();
thermo_k_2 = thermocouple_2.readCelsius();
}
void SERIALCOM() {
Serial.print(traction1);        //read in Newton
Serial.print(",");
Serial.print(reading_2);        //read in grama
Serial.print(",");
Serial.print(thermo_k_1);       //read in Celsius
Serial.print(",");
Serial.print(thermo_k_2);       //read in celsius
delay(500);
}
```

Appendix B

B. Technical Drawings

B.1. Pulsejet

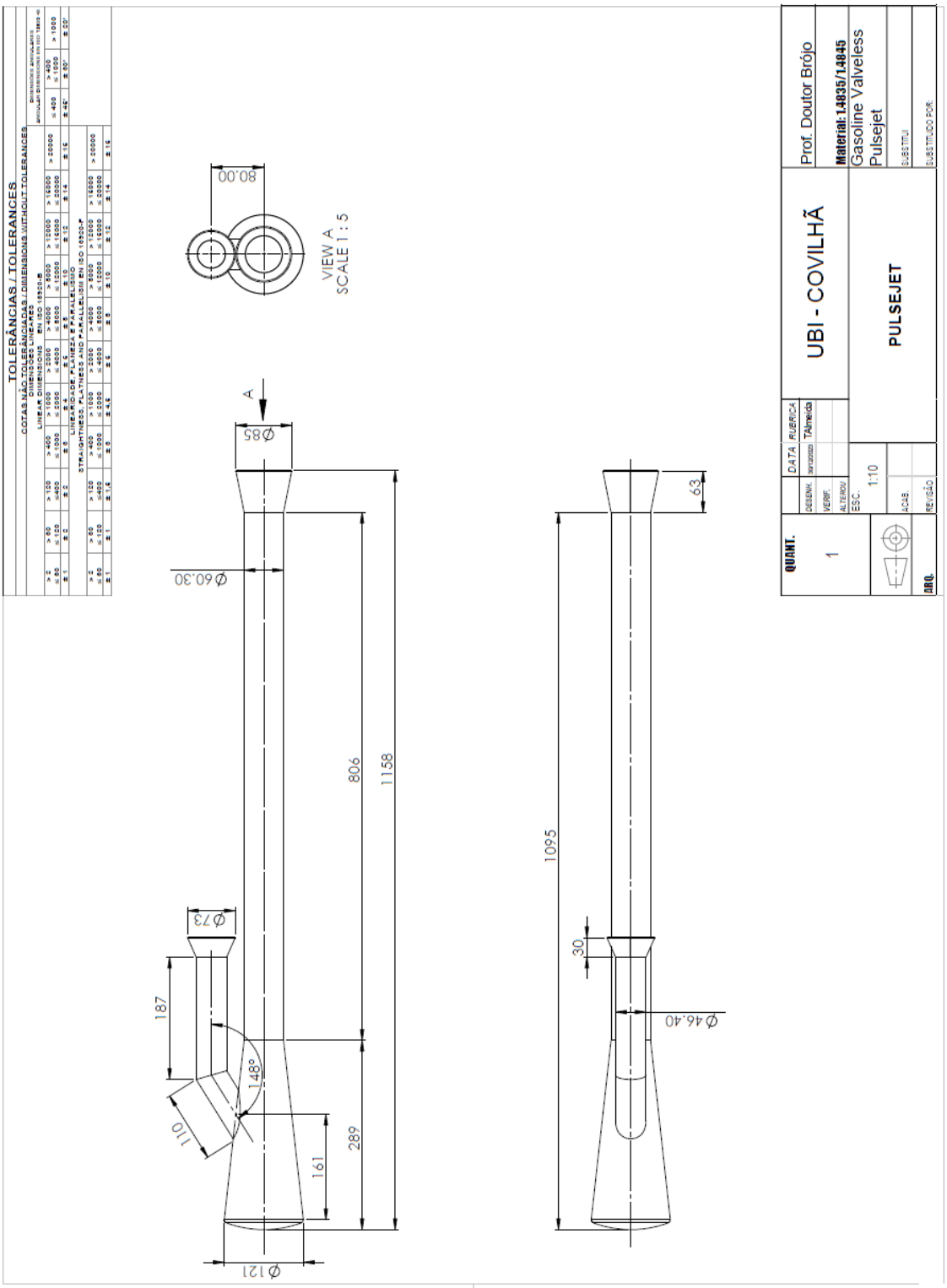

B.2. Admission Flare

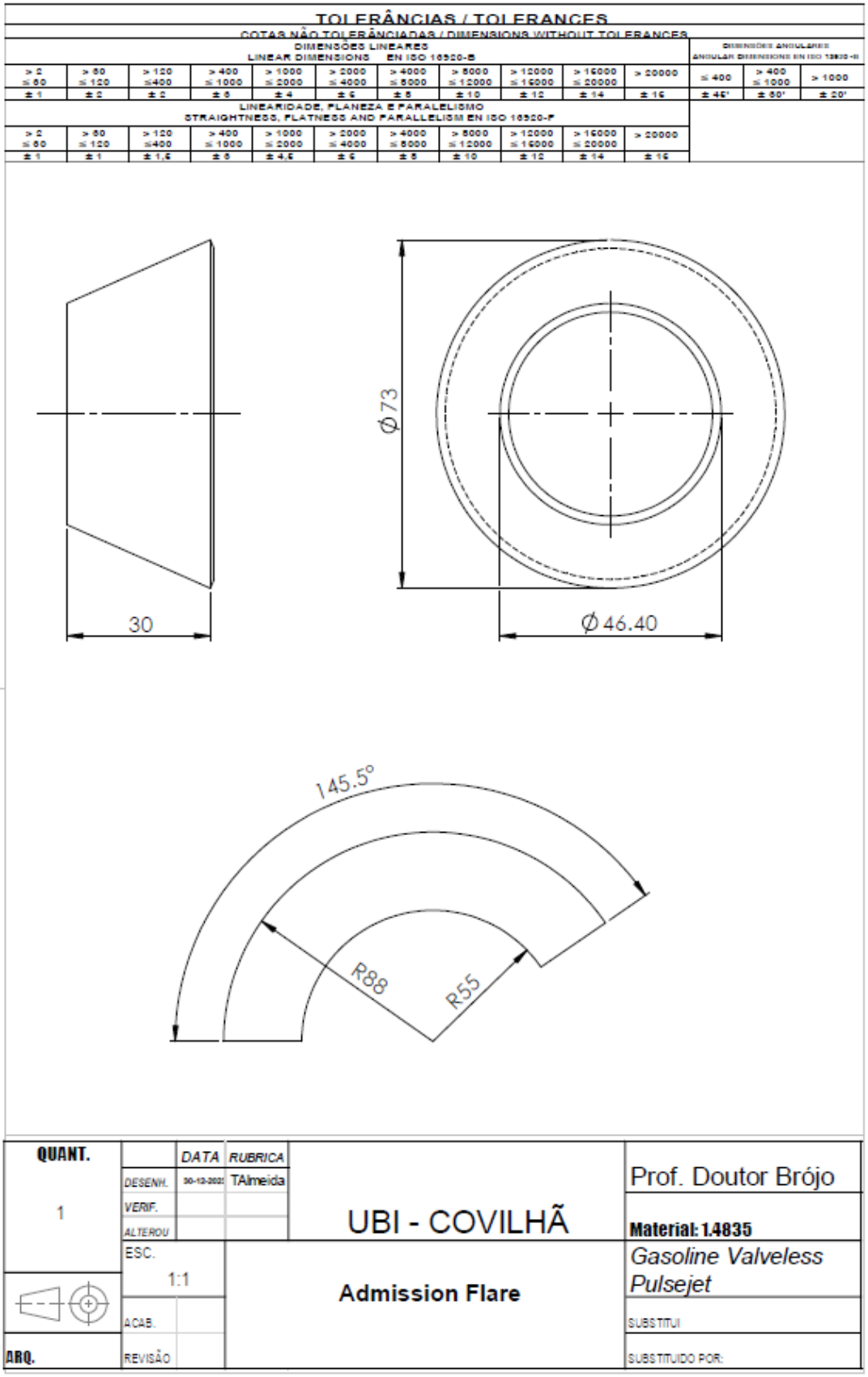

B.3. Exhaust Flare

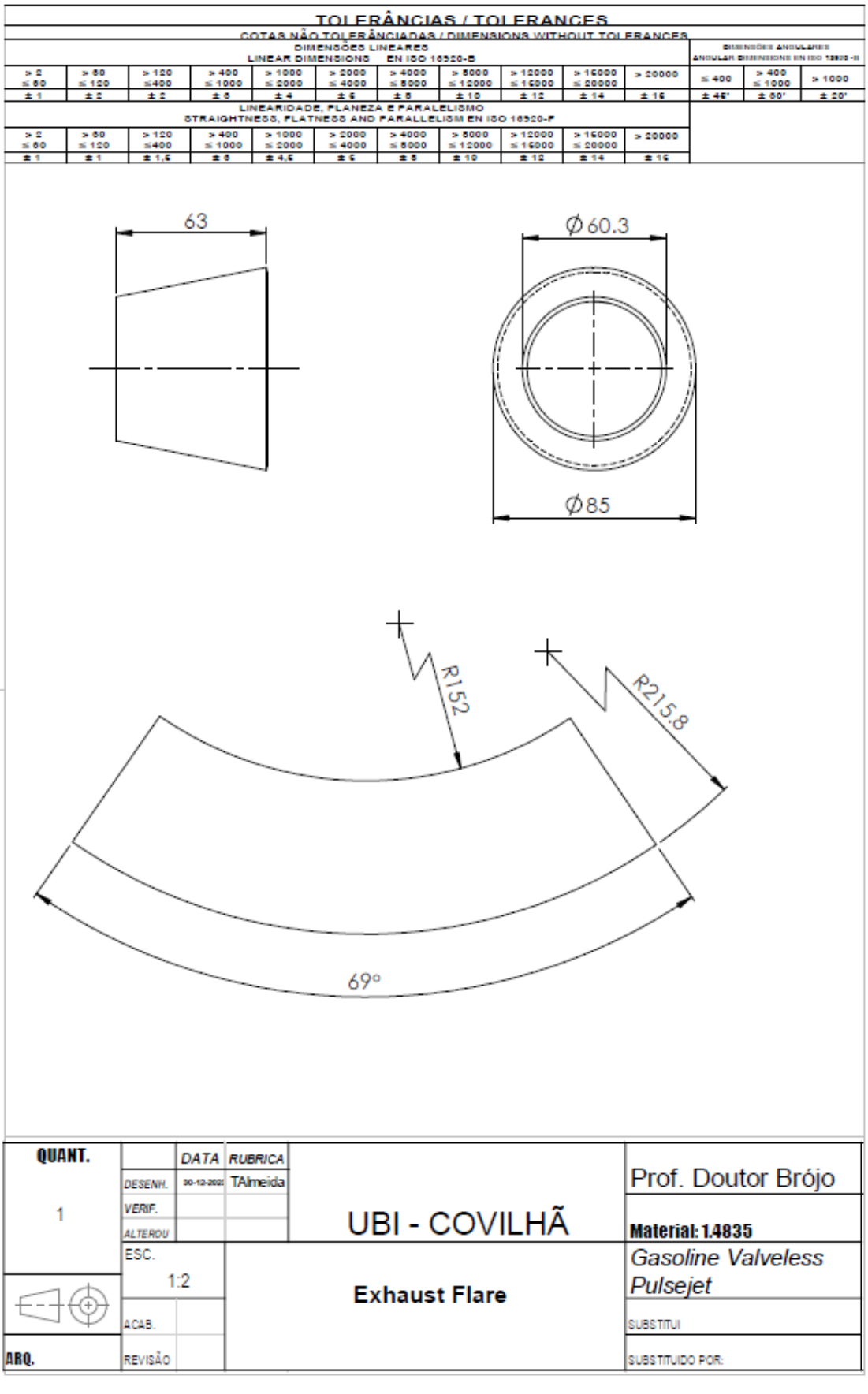

B.4. Combustion Chamber

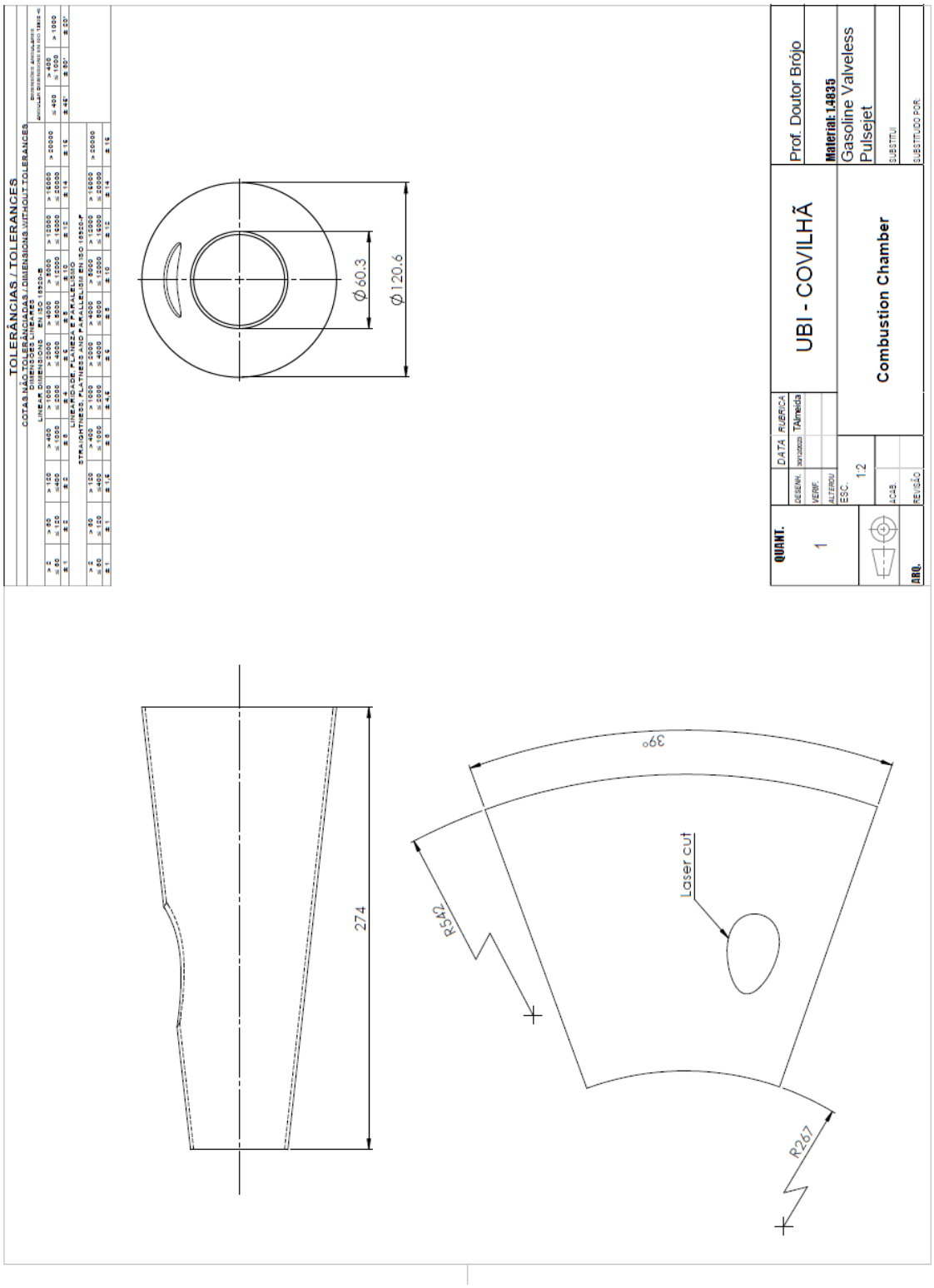

Appendix C

C. Eletronic Device

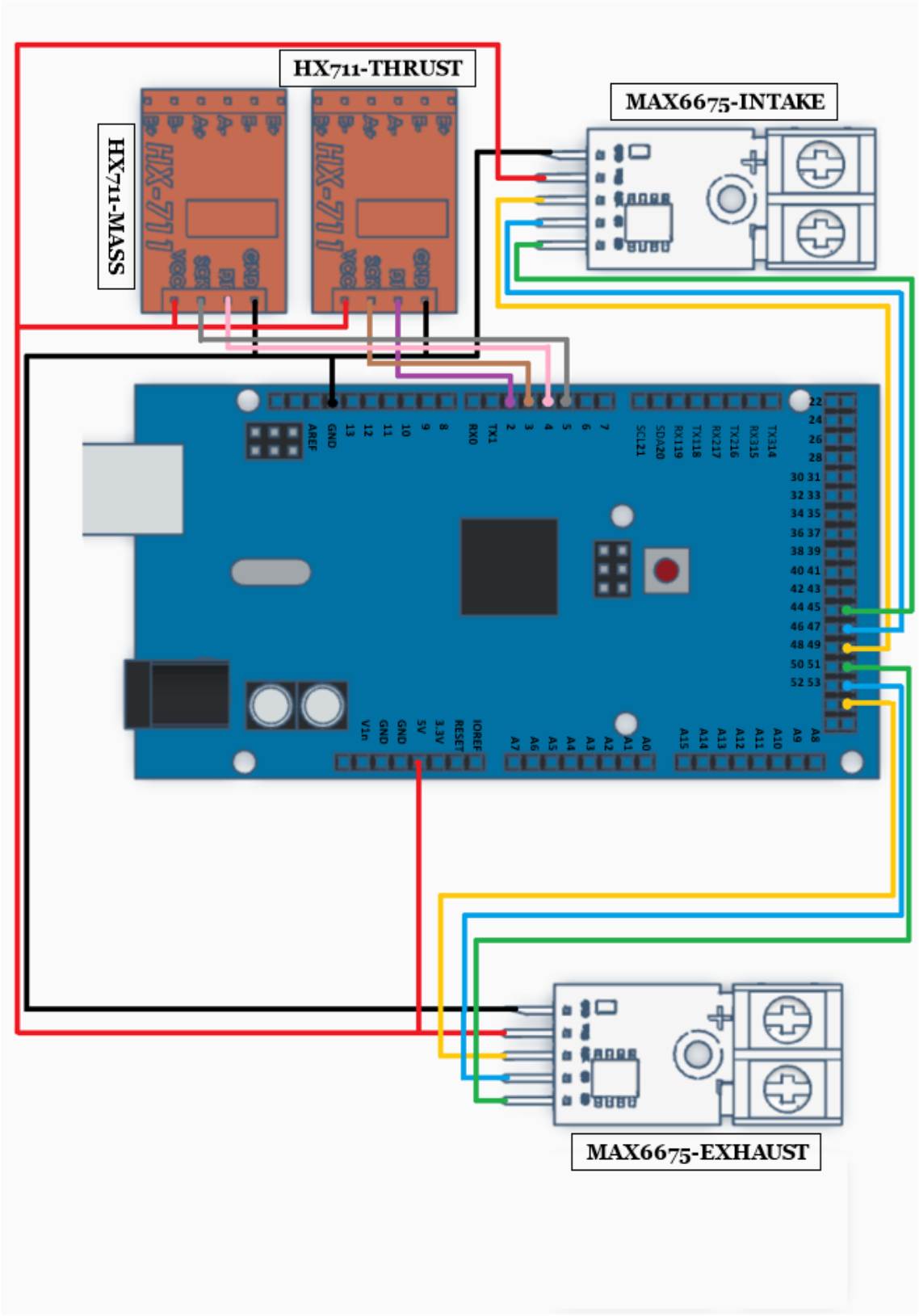

Appendix D

D. Steel Technical Data Sheets .

D.1. Stainless Steel 1.4845

SANDVIK

CERTIFICATE

A03/Z02
No. A/21-981047 **Rev** 00
Date 2021-11-10 **Page** 1/2

83287

A02/Z03
INSPECTION CERTIFICATE acc to
EN 10204 3.1

INSPECTION STAMP
QA-TUBE

A06
ARSOPI-IND METALURGICAS
ARLINDO S PINHO, SA
APARTADO 10 RELVA - VILA CHA
3730-954 VALE DE CAMBRA
PORTUGAL

Customer References A07
ENC NR 200004918
Customer order 2021-11-09

280-00154 ARSOPI

Sandvik References A08

Order No.	Subs No.	SMT Dispatch note
578125	704189	49726/54

SMT No.	C.Code
300-37523	53

Material description B01/B04
SEAMLESS STAINLESS HOT FINISHED
TUBE FOR HIGH TEMPERATURES

Metallurgical process C70
Electric furnace

Steel/material Designations B02

Sandvik	AISI
7RE10	TP310S/TP310H
UNS	**EN no**
S31008/S31009	1.4845

Technical requirements B03
ASTM A-312-19/ASME SA-312-ED-19
EN 10297-2, EN 10216-5 TC1 (Testings)
NACE MR0175/ISO 15156-3:-2015

EXTENT OF DELIVERY B07-B13

It	Product designation	Heat	Lot	Pieces	Kg	M
01	THR-E-7RE10-11/2-SCH40 48.26 X 3.68	561495	37995	1	29.0	6.88
			Total	1	29.0	6.88

TEST RESULTS
Chemical composition (weight%)

Heat	C	Si	Mn	P	S	Cr	Ni	Mo	N
561495	0.048	0.40	1.23	0.023	<0.0005	24.11	20.14	0.23	
561495									0.050

Tensile test at room temperature

	Yield strength MPa	MPa	Tensile strength MPa	Elongation %	%
Lot	Rp0.2	Rp1.0	Rm	A	2"
37995	325	353	589	42	39

Quality assurance - Helen Jämtemyr / QA-manager A05/Z02
MTC Service / Certificates

A01 AB SANDVIK MATERIALS TECHNOLOGY Reg No. 556234-6832 VAT No. SE556234683201
SE-81181 SANDVIKEN SWEDEN www.materials.sandvik mtc_service.smt@sandvik.com

Hardness test

Lot	Min HRB	Max HRB
37995	73	73
	68	69

Grain size

Lot	
37995	4.0
	4.0

Following controls/tests have been satisfactorily performed:
- Flattening test.
- Flaring test
- 100% PMI-test.
- Leak test: Eddy current test acc to ASME SA-999, EN ISO 10893-1
- Visual inspection and dimensional control.

Heat Treatment:
Solution annealed and quenched.

Marking:
SANDVIK ASTM A312 ASME SA312 TP310S TP310H EN 10297-2 1.4845 HFD SML ET 48.26 X 3.68 MM 1 1/2 SCH 40S HT 561495 SS LOT 37995 *QA-TUBE*

The raw material is free from radioactive contamination.

Material free from mercury contamination.

The number of tests are based on the size of the manufacturing lot before cutting to finished lengths.

The delivered products comply with the specifications and requirements of the order.

The material is manufactured according to a Quality system, approved and registered to ISO 9001:2015.

No unauthorized alterations. The contents of this Inspection Certificate may not be modified or revised in any way without the prior written approval of Sandvik Materials Technology. Unauthorized alterations to the Inspection Certificate, including introduction of false, fictitious or fraudulent statements or entries, may be punishable by fines, imprisonment, or both. This Inspection Certificate may be copied only in the manner and for the purposes specified in Section 6 of EN 10204:2004. Contravention of this notice will be prosecuted to the fullest extent of applicable law.

The certificate is produced with EDP and valid without signature.

D.2. Stainless Steel 1.4835

J3739

outokumpu
high performance stainless steel

CERTIFICATE - ZEUGNIS - CERTIFICAT
EN 10204-3.1
2355289-EN

Invoice No. / Rechnung Nr. / N° de facture: 6610/1000418955
Page / Seite / Page: 1/1

Business Unit / QCM	Date / Datum / Date	Load, Ladung, Charge No	Acknowledged ID, Bestätigung, Commande ID
Avesta Works / Johan Nordström	27-Jan-2016	PT/129144	6610/300369372

Your ref, Ihre Ref., Votre ref: EF-24011

Requirements, Anforderungen, Exigences: EN 10095 (03.99) EN ISO 9445

Buyer, Besteller, Acheteur:
INACEINOX-IND. DE EQUIP. INOX.,S.A.
RUA DE VALE PEREIRAS 724
3730-901, VALE DE CAMBRA
PORTUGAL

Consignee, Empfänger, Lieu de livraison:
INACEINOX-IND. DE EQUIP. INOX.,S.A.

Mark of Manufacturer / Zeichen des Lieferwerkes / Signe de producteur	Process / Erschmelzungsart / Mode de fusion	Inspector's stamp / Zeichen des Sachverständigen / Poinçon de l'expert	Grade, Werkstoff, Nuance
outokumpu	E+AOD	AJA	Outokumpu 253 MA 1.4835

Product, Erzeugnisform, Produit:
Stainless Steel Cold Rolled, Coil-Plate
finish 2E, pickled, cut edge

Line / Reihe / Ligne	Item / Position / Poste	Heat-Lot No / Schmelze-Lot Nr / Coulée n° - Lot No	Size / Abmessungen / Dimensions	Pieces / Stückzahl / Nombre	Quantity / Unit / Menge / Einheit / Quantité / Unité
1	9	554223-001	2,00 X 1500 X 6000 mm	1	143 KG

Chemical composition – Chemische Zusammensetzung – Composition chimiques

	C	Si	Mn	P	S	Cr	Ni	Nb	Cu	Co	N	Ce
Heat	.089	1.63	.49	.026	.001	21.20	10.83	.004	.21	.230	.169	.04

Radioactive contamination check acc. IAEA recommendations: Approved

Test results – Prüfergebnisse – Results dessais (1N/mm² = 1 MPa) F = Front – Anfan – Debut B = Back – Ende – Fin T = Transverse – Quer – Travers

Test Ref		Temp °C	RP 0.2 N/MM2	RP 1.0 N/MM2	RM N/MM2	A80 %	GRAIN SIZE
Min		+20	310	350	650	37	
Max					850		
F	T	+20	402	478	724	48	7.5
B	T		395	460	711	52	

Grain size acc to ASTM E112: Approved
Heat treatment / Solution annealed: Material temperature 1120 °C / Quenched (forced air + water)
Steel grade verification (PMI-spectroscopic): Approved
Marking, visual insp. and gauge measurement: Approved

Outokumpu Stainless AB
Business Unit Special Coil
BOX 74, S-774 22 AVESTA
SWEDEN
Regoffice: Stockholm SWEDEN, Regno: 556001-8748

Telephone: + 46 (0)226 811 73
Fax: + 46 (0)226 816 46
V.A.T no: SE556001874801

This material is found to comply with order requirements

Joakim Johansson
Authorized Inspector

TÜV NORD ISO 9001